Chemical Geology 656 (2024) 122106

Contents lists available at ScienceDirect

Chemical Geology

journal homepage: www.elsevier.com/locate/chemgeo

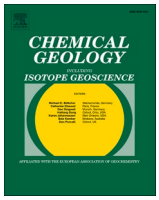

Invited review article

The impact of Himalayan-Tibetan erosion on silicate weathering and organic carbon burial

Peter D. Clift [a,b,*], Tara N. Jonell [c], Yifan Du [a], Thomas Bornholdt [b]

[a] Department of Earth Sciences, University College London, 5 Gower Place, London WC1E 6BS, UK
[b] Department of Geology and Geophysics, Louisiana State University, Baton Rouge, LA 70803, USA
[c] School of Geographical and Earth Sciences, University of Glasgow, Glasgow G12 8QQ, UK

ARTICLE INFO

Editor: Oleg Pokrovsky

Keywords:
Weathering
Erosion
Orogeny
Climate change
Himalaya
Organic carbon
Ocean drilling

ABSTRACT

Cenozoic mountain building in Asia has been proposed as an important control over global climate by atmospheric CO_2 drawdown through silicate weathering and burial of organic carbon (OC) offshore. Because Asian submarine fans represent the most complete record of Asian orogenic erosion and weathering over the Cenozoic, evaluation of sediment major element chemistry and OC content can be used to estimate CO_2 sequestration rates driven by silicate chemical weathering and OC burial. From deep-sea fans in the Indian Ocean and South China Sea, weathering rates are calculated by comparison of weathered sediment to initial bedrock source compositions and then integrated with deposited volumes to derive the first regional weathering budget for India-Asia collision over the last ~25 m.y. Results indicate the Indus is more important than previously recognized before and during the middle Miocene in sequestering CO_2 (~76% of Asian total at 16–14 Ma). This in part reflects the more reactive mafic and ultramafic bedrock sources compared to the largest and major east Himalayan drainage, the Ganga-Brahmaputra, but also greater erosional flux from the onshore Indus drainage at that time. This regional synthesis further concludes that OC burial only represented a minority (20–25%) of the regional carbon budget but became more important after 17 Ma, peaking at ~38% after ~3 Ma. CO_2 sequestration rates increased from 17 to 15 Ma, coinciding with the Miocene Climatic Optimum, and remained mostly steady in Asia from ~15–5 Ma as the climate cooled. Only one of three possible sediment flux models for the Bengal Fan predicts increased CO_2 consumption rates after 15 Ma and, even then, only predicts steady rates from 11 to 5 Ma. The timing of changes in CO_2 consumption rates are not consistent with Asian orogenic silicate weathering acting as the dominant control over late Cenozoic atmospheric CO_2.

1. Introduction

The evolving climate of Earth is strongly influenced by changing concentrations of atmospheric greenhouse gases (Crowley and Berner, 2001). The concentration of atmospheric CO_2, which is the most important forcing gas over geological timescales, is balanced between outputs from the solid Earth ('sources') against processes that sequester CO_2 from the atmosphere and store it long-term in the geological record ('sinks')(Berner and Berner, 1997). Source and sink processes operate over a range of timescales, spanning from decadal periods to 100 s of millions of years. CO_2 is supplied to the atmosphere primarily via subduction-related or mid ocean ridge magmatism from the mantle. Falling rates of seafloor spreading during the Neogene have been implicated in slowing the rate of outgassing (Herbert et al., 2022). Sinks include carbon deposition as carbonate sediments, burial of organic carbon (OC) (Galy et al., 2007), and calcite mineralization of the oceanic lithosphere (Alt and Teagle, 1999; Bach et al., 2003) followed by subduction into the mantle, or storage in the lower continental crust (Touret, 1992). Of all these the role that chemical weathering plays has been most strongly debated and continues to be a subject of research.

Chemical weathering has repeatedly been proposed as a buffer of atmospheric CO_2 levels (Walker et al., 1981), including both oceanic seafloor weathering (Caldeira, 1995; Brady and Gíslason, 1997; Coogan and Gillis, 2013) and terrestrial weathering of silicate minerals. In particular, it has been hypothesized that the growth of high topography in Asia following probable Eocene collision of India with Eurasia (de Sigoyer et al., 2000; Najman et al., 2010; Bouilhol et al., 2013) was a critical component of this global climate evolution (Raymo and

* Corresponding author at: Department of Earth Sciences, University College London, 5 Gower Place, London WC1E 6BS, UK.
E-mail address: peter.clift@ucl.ac.uk (P.D. Clift).

https://doi.org/10.1016/j.chemgeo.2024.122106
Received 6 December 2023; Received in revised form 11 March 2024; Accepted 16 April 2024
Available online 21 April 2024

Ruddiman, 1992). This study presents the first, integrated regional silicate weathering synthesis that greatly supersedes earlier work based on single depocenters. Through this synthesis, we revisit the classic hypothesis that suggests increased chemical weathering fluxes from the growing and rising Himalaya are responsible for global cooling over the last 25 million years. We further evaluate this argument by constructing the first total weathering flux associated with Himalayan mountain building by integrating regional organic carbon burial records with revised chemical weathering flux estimates, and evaluate this combined CO_2 budget in context to trends in Earth climate over the Neogene.

2. Estimating CO_2 sequestration

Increases in the relative reactivity of bedrock have been proposed to reconcile evidence for decreasing Cenozoic atmospheric CO_2 in spite of isotopic evidence for an invariant global silicate weathering flux (Kump and Arthur, 1997). This has been argued to mean that other regions may significantly contribute to the global CO_2 budget and not just the Himalayan erosion-induced silicate weathering (Caves et al., 2016). Consequently, the focus of weathering research pivoted toward stronger consideration of tropical arc and ophiolite complexes (Jagoutz et al., 2016; Macdonald et al., 2019; Park et al., 2020; Bayon et al., 2023; Martin et al., 2023) that are characterized by more reactive, soluble Ca- and Mg-rich mafic and ultramafic rock compositions (Dessert et al., 2001). Nonetheless, the sheer volume of material derived from the Himalaya, plus the fact that this collision zone exposes mafic and ultramafic lithologies, and transited through tropical latitudes for a significant portion of its paleogeographic history (van Hinsbergen et al., 2012) merits that any comprehensive global Cenozoic CO_2 budget must involve consideration of the India-Eurasia collision and the remnant Himalayan orogen today.

Numerous studies have attempted to test the uplift-erosion-weathering model, both directly and indirectly. Richter et al. (1992) used seawater Sr isotopes to argue that Himalayan weathering was of the right magnitude and timing to have dominated the global budget since the onset of collision. A similar conclusion was reached using Li isotopes sensitive to continental weathering (Misra and Froelich, 2012). The issue remains contentious as Be isotopes have been used to argue for stable erosion and weathering rates since ~12 Ma (Willenbring and von Blanckenburg, 2010), although this is not universally accepted.

Total silicate chemical weathering fluxes may be calculated from the volumes and their degree of alteration of sediment eroded from the orogen, following the quantitative approach of France-Lanord and Derry (1997). That approach focused on changes in Mg and Ca concentrations, and to a lesser extent Na and K, between source bedrock and derived sediment. If deposited volumes can be constrained, and the amount of CO_2 consumed per unit weight of sediment (ΔCO_2) calculated, then estimates of CO_2 consumption can be made. Such estimates for three of the major river systems draining the Himalaya and Tibetan Plateau (Indus, Mekong and Pearl rivers; Fig. 1) and their offshore deposits showed no increase over the Neogene (Clift and Jonell, 2021a). However, that study had several shortcomings because of its focus on silicate weathering fluxes only, with no consideration for the chemical weathering of carbonates or other minerals. CO_2 release during erosion of high and actively uplifting mountains has become increasingly recognized. Sulfuric acid formed by weathering of petrogenic pyrite can react with carbonate to effectively release CO_2 to the atmosphere (Spence and Telmer, 2005; Calmels et al., 2007; Li et al., 2008; Torres et al., 2014). Furthermore, it is generally well-recognized that weathering of Tethyan Himalayan carbonates could have at least partly counteracted any CO_2 consumption produced by silicate weathering in other parts of the orogen. Nonetheless, geochemical modelling of sulfide weathering has also highlighted feedbacks on atmospheric oxygen concentrations associated with the organic carbon (OC) cycle. While an increase in sulfide weathering may first lead to CO_2 release, it is then followed by a greater decrease in CO_2 (Maffre et al., 2021). Addressing this issue is beyond the scope of this work, not least of which is the lack of a robust proxy that can constrain past carbonate weathering.

The products of carbonate and petrogenic OC weathering reactions are gases and liquids that are not preserved in the sedimentary record; thus making reconstruction of these weathering processes and their products in the past difficult. Rates of modern carbonate, silicate, and petrogenic OC weathering have been quantified in part by study of dissolved loads in rivers today. Weathering of petrogenic OC has been estimated to approximate or even exceed CO_2 drawdown induced by silicate weathering (Hilton et al., 2021; Zondervan et al., 2023), if not that by OC burial. Under faster physical erosion, the rate of petrogenic OC oxidation would also be expected to increase. However, release of CO_2 by this process may be counterbalanced by CO_2 sequestration via rapid contemporary OC burial offshore, such as documented in Taiwan

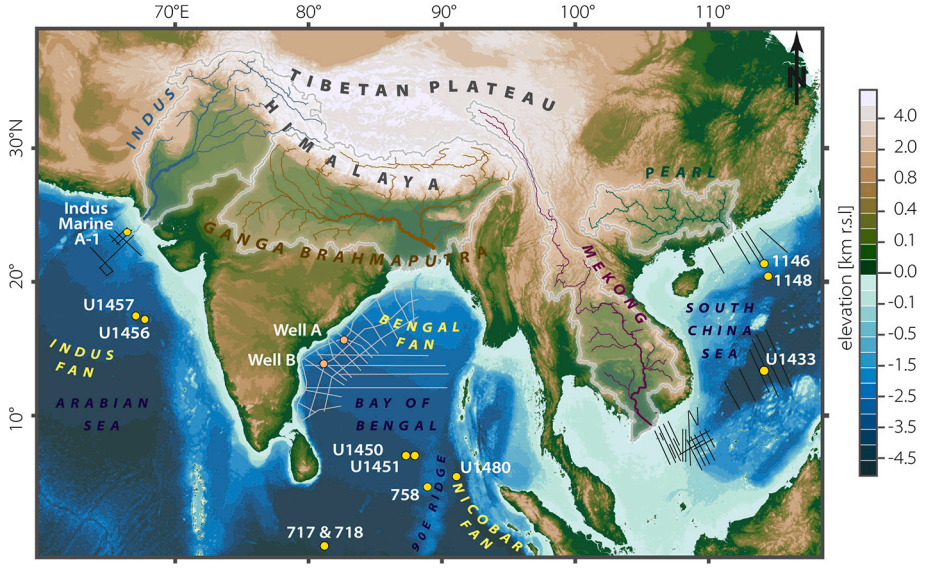

Fig. 1. Digital terrainmap of South and SE Asia showing the location of the drill sites and seismic profiles used to estimate mass flux rates from the continent. Black lines are from Clift (2006), while gray lines show the coverage from Krishna et al. (2016). Elevation data derived from the 15-arc *sec* HydroSHEDS v1 dataset (Lehner et al., 2008; Lehner and Grill, 2013) for onshore gridded elevations, with 15-arc sec GEBCO 2019 gridded bathymetry (GEBCO Compilation Group, 2019). Rivers and basins modified from HydroRIVERS, with river line width proportional to upstream catchment area.

(Hilton et al., 2014). Although modern river water can often provide a detailed snapshot of present-day processes, modern river chemistry is not necessarily representative of ancestral river chemistry nor regional weathering rates over longer periods of geologic time. In this case, we compared the result from our studied ancient sediments and modern rivers.

Estimating CO_2 consumption is further complicated by the role of diagenesis, often called reverse weathering (Dunlea et al., 2017; Isson and Planavsky, 2018). After its deposition on the seafloor, sediment is progressively transformed from loose material into rock by compaction and precipitation of diagenetic secondary minerals. The formation of diagenetic minerals, such as smectite clay, can release CO_2 as Na and K are fixed into the clay mineral structure (Mackenzie and Kump, 1995). Hypothetically, smectite abundance could be used to quantify the degree of diagenesis but would require the discrimination of primary detrital smectite from diagenetic secondary smectite. While this can be done, it is difficult to constrain for large volumes of sediment deposited in deep-sea fans. K and Na are lost from eroded rock fragments because of weathering during transport (consuming CO_2), but can be added again during secondary smectite formation (releasing CO_2). Measuring sediment alkali element concentrations only allows for estimates of the net change in K and Na concentrations and thus a net CO_2 loss or gain. The relative influence of reverse weathering may be inferred when alkali element concentrations in sediment are enriched relative to potential source rock compositions. If geochemical changes in deposited deep-sea sediment were only attributed to silicate chemical weathering, it would not be possible for eroded and weathered sediment to be fresher than its parent material, as is sometimes observed. Therefore, enrichment of alkali elements relative to source rock values nullifies the assumption that only silicate weathering affected concentrations and requires that reverse weathering (diagenesis) be considered.

3. Making a silicate weathering budget for high Asia

Asian submarine fans represent the most complete record of Asian orogenic erosion and weathering over the Cenozoic. Sedimentation in the Indus Fan (IF) is estimated to have begun in the Eocene (Clift et al., 2001). Drilling in the Bengal Fan (BF) revealed at least 27 m.y. of sedimentation (Ali et al., 2021), although geophysical surveys point to an origin in the Early Eocene (Curray et al., 2003). The Mekong River commenced sedimentation in its present location after ~8.5 Ma (Liu et al., 2017), while the Nicobar Fan, essentially an eastern extension of the BF, dates from ~11 Ma (McNeill et al., 2017a). The Pearl River is estimated to have initiated at ~30 Ma (Jin et al., 2022).

All sediment in the submarine fans is transported through terrestrial environments and, while some are preserved in those settings, the vast majority of sediment is stored in the ocean. The only significant onshore basin is the Himalayan foreland basin, estimated at 1.2×10^6 km^3 (Clift et al., 2001). The foreland basin can be considered to be permanently filled, at least during the time interval considered here because sedimentary facies over this interval are overwhelmingly fluvial (Najman, 2006). Himalayan foreland basin sediments are progressively offscraped and cannibalized or underthrust as convergence continues. The current volume of the foreland is ~7% of the total volume estimated to be held in the oceanic depocenters (Clift et al., 2001). Therefore, the total amount of sediment eroded from the sources and not included in the budget presented here is quite modest. The proportion of the current sediment flux to the ocean recycled from eroded foreland sedimentary rocks is <15% (Lavé and Avouac, 2001), meaning that fluxes in the Himalayan foreland basin contribute only modest uncertainties to the regional weathering budget. Weathering fluxes associated with the foreland basin, whether involving younger floodplain or recycled older accreted strata (e.g., Siwalik Group), is included in the total weathering estimate presented here.

We here estimate the amount of CO_2 consumption by silicate weathering and OC burial. CO_2 consumption driven by silicate weathering in the Indus, Mekong and Pearl river basins has previously been estimated by Clift and Jonell (2021a), but here we recalculate these values to partly account for reverse weathering processes and newly compiled OC data. The previous study used the Upper Continental Crust (UCC) values from Rudnick and Gao (2003) as the bedrock source composition for the Pearl and Mekong rivers, but artificially enhanced bedrock source K concentrations because of higher K concentrations in weathered sediment. This was done because the original UCC value implied that the sediment was fresher than the original bedrock, which would be impossible. Yet the contributions of reverse weathering (diagenesis) on sediment elemental concentrations was not considered. In this revised budget, we apply the original UCC compositions and do not correct the K/Al ratios to force a net depletion. This partly corrects for the CO_2 release driven by reverse weathering. Our estimates here further account for the changing provenance of sediment, and thus the evolving chemical compositions, of transported sediment reaching the deep-sea fans over time. Weathering estimates for the IF were adjusted for shifting provenance recorded by the onshore Indus River, especially accounting for the compositional differences between the more continental felsic sources of the Himalaya and more mafic sources in the Indus Suture Zone and Karakoram. The relative erosional contributions at any one time from each of the bedrock source end members were calculated from bulk sedimentary Nd isotope values based on average ε_{Nd} values of −5.0 documented for the Indus Suture Zone and − 15.7 for the Himalaya (Clift et al., 2019). The UCC composition of Rudnick and Gao (2003) was used for the Himalayan bedrock while the Indus Suture Zone bedrock composition was from Clift and Jonell (2021a) who compiled a representative endmember from the GEOROC database.

The revised budget presented here now includes estimates for the largest catchment, the Ganga-Brahmaputra, and its sediment largely stored in the BF in the Bay of Bengal (BoB) (Fig. 1). Prior estimates omitted the BF due to the lack of a reliable mass flux budget constrained by volumetric estimates via seismic stratigraphy. This was unfortunate because the BF accounts for ~50% of all the preserved Neogene sediment in the Asian marginal seas (Clift, 2002). While it might be expected that its weathering history might be like its neighboring basins (i.e., Indus), it is not always sensible to assume that is the case. Prior work from the distal BF implied a reverse relationship between climate and chemical weathering in this basin might exist. Greater chemical weathering was recorded during drier intervals rather than less, as also observed across the Indus system (France-Lanord et al., 1993; Clift et al., 2008). This relationship likely reflects slower transport during drier times because of reduced discharge. The resulting longer sediment residence times onshore can result in greater net degree of sediment alteration than during wet intervals, even if the rates of weathering are comparatively slower.

Given the volumetric significance of the BF and its potential contribution to regional CO_2 consumption, it is essential to constrain the magnitudes of and trends in total chemical weathering fluxes and OC burial in this system. OC burial in the BF was argued to be critical in sequestering CO_2 and, consequently, act as an essential component driving cooling at the global scale (France-Lanord and Derry, 1997). However, previous estimates of OC burial and silicate weathering were based either on data from a single drilling expedition in the southern BF through Ocean Drilling Program (ODP) Leg 116 (Fig. 1), or inferred from differences in water isotopic compositions between the northern and southern BoB (Song et al., 2023). It remains debatable whether these data are truly representative of regional fluxes, in addition to the limited spatial resolution and volumetric constraints by regional seismic stratigraphy.

Significant progress has been made in expanding sampling of the BF since ODP Leg 116, because of coring in the BoB and neighboring basins undertaken from 2014 to 2016 by the International Ocean Discovery Program (IODP). This campaign targeted the South China Sea, BoB, and Arabian Sea (Clift et al., 2022). This work now allows a substantially improved estimate of Neogene carbon burial and CO_2 sequestration to

be made for South Asia. Details concerning how the sedimentation rates are estimated are provided below, including three possible models for the BF based on three approaches to calculating flux rates: from (1) limited regional seismic data; (2) hemipelagic clastic sedimentation rates on Ninety East Ridge; and (3) clastic sedimentation rates comparable to the IF.

4. Estimating the carbon budget

4.1. Age control

Any carbon budget requires age control and our age models for each site are derived from the shipboard reports, which have sometimes been updated, e.g., IODP Sites U1456 and U1457 (Routledge et al., 2020). When possible, we use the integrated results of nannofossil and foraminiferal zones with magnetic reversals to develop age models; but when these are in dispute, we defer to defined nannofossil zones. Biostratigraphic ages were converted into a numerical age using the timescale of Gradstein et al. (2020).

4.2. Organic carbon budget

We reconstruct a Cenozoic OC burial history using sediment OC concentrations determined by scientific ocean drilling expeditions. After determining a time-averaged OC (%) concentration from an interval of sediment, the total OC preserved in each fan can be calculated if the rate of delivery of sediment to each depocenter is constrained. Because linear sedimentation rates at a single site are not accurate proxies for the total mass flux into any given basin (Métivier et al., 1999), three-dimensional reconstructions of sediment accumulation reconstructed from regional seismic reflection profiles are used to estimate sediment flux and OC burial through time (Clift, 2006) (Fig. 1). These profiles are tied to industrial wells and generally have a low temporal resolution but can provide robust long-term estimates of sediment flux. Because the temporal resolution of OC content is much greater in each well (higher sampling resolution) than the seismically derived mass flux (Fig. 2), we use time-averaged OC values for each seismic package derived from all wells in each submarine fan system. This results in a long-term average rate of OC burial that is the focus of this work. The greatest uncertainties in our budgets are related to the errors calculated from seismic velocities that introduce significant uncertainties into the time-depth conversion and, therefore, into the total mass accumulation rates. We conservatively estimate ±20% uncertainty, following the approach of Clift (2006).

We note that some of the total sediment OC includes petrogenic OC derived from eroded onshore sources. This petrogenic material is recycled from the sedimentary record and not derived directly from recently-living flora or fauna. Petrogenic OC contributes very little to the total OC in the BF, as observed in Holocene at least (Galy et al., 2007; Galy et al., 2008). Petrogenic OC in modern-day river loads of the Indus and Mekong account for ~7% of the total OC in the Mekong River, with as much as 20% of total OC in the Indus River (Galy et al., 2015). Estimating how much petrogenic OC contributed to total sediment OC in the past is more problematic given that it will vary from basin to basin as the provenance of sediments change and as the contributing onshore carbon sources to sediment also evolve. Thus, a precise correction is impossible for petrogenic OC but it has been suggested that a ± 20% petrogenic OC contribution to total OC would be a plausible and conservative range (Galy et al., 2015). Furthermore, given that we use total OC burial to calculate rates of CO_2 sequestration, our calculations innately overestimate the total CO_2 consumption given the contribution from petrogenic OC to the total.

4.3. Bengal fan sediment budget

The BF is less well surveyed than its neighbors in terms of published seismic reflection coverage of offshore sediment. Consequently, we estimate the mass flux into this basin using three different but plausible approaches as applied to the estimated volume (7.19×10^6 km^3) of Neogene BF sediment (Clift et al., 2001). In Model 1 we apply the sediment budget of Krishna et al. (2016) that relies on volumes calculated from regional seismic reflection profiles tied to industrial wells for the NW BoB (Figs. 1 and 3A). However, it is important to note that the locations of the Krishna et al. (2016) wells (and seismic data) are heavily

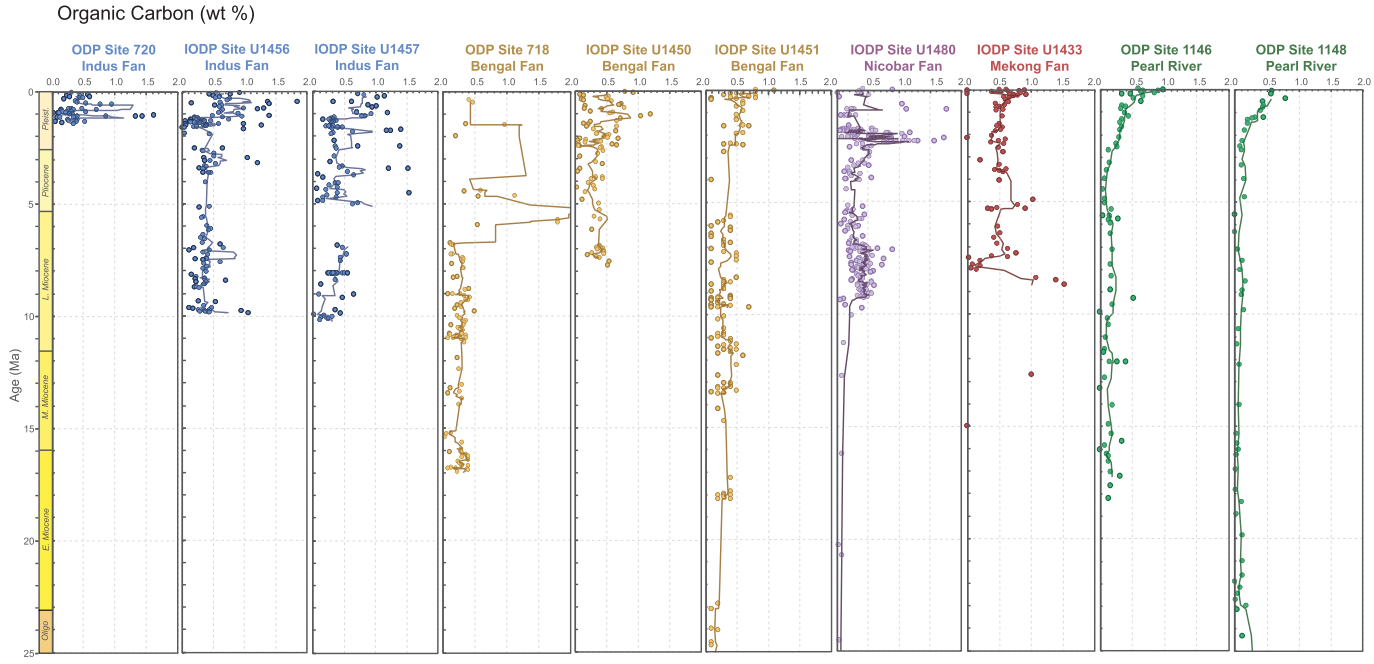

Fig. 2. Temporal variations in the organic carbon (OC) content at the scientific drilling sites used in this study. Data are from the shipboard reports referenced in the main text. Black line shows 5-point running average. Data taken from the mass wasting deposit drilled at IODP Sites U1456 and U1457 are not included, as this does not represent flux from the Indus River system.

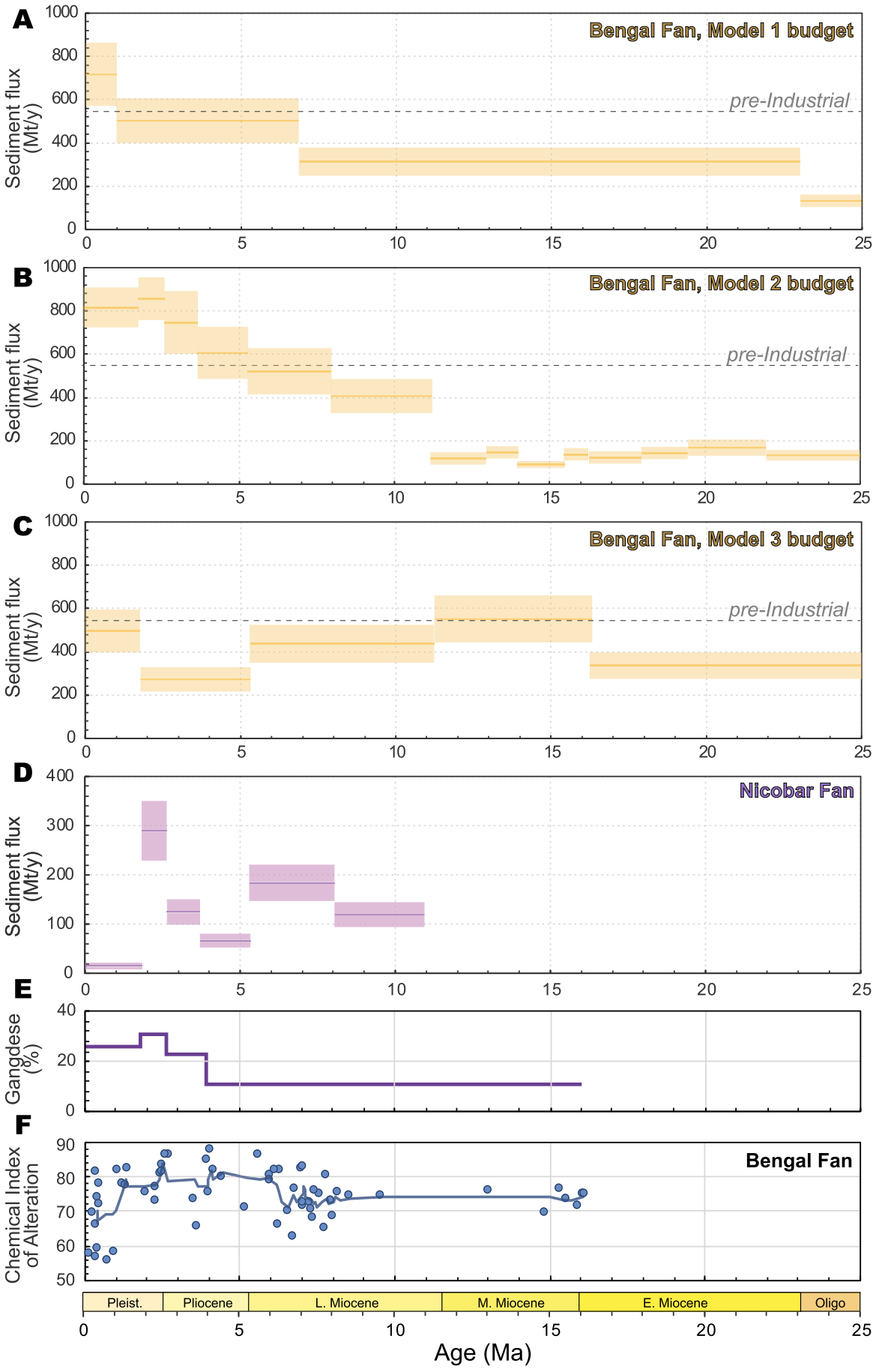

(caption on next page)

Fig. 3. Sediment mass flux budgets for the BF based on A) regional seismic from western Bay of Bengal (BoB)(Krishna et al., 2016), B) clastic sedimentation rates at ODP Site 758 (Ali et al., 2021), and C) mirroring rates of change in the Indus Fan (IF)(Clift, 2006). D) Rates for the Nicobar Fan proxied by sedimentation at IODP Site U1480 (McNeill et al., 2017b). E) Temporal changes in the proportion of Gangdese supplied sediment to the BF, F) Temporal variations in Chemical Index of Alteration for the Bengal Fan (BF).

influenced by sediment delivery from peninsular India, as well as that from the Ganga-Brahmaputra delta. This cautions the direct use of these NW BoB wells as a wholly representative proxy for eastern Himalaya fluxes to the BF via the Ganga-Brahmaputra. Nonetheless, the NW region offers the highest seismic resolution for a portion of the BF, even if it is not representative of sedimentation rates across the entire BF.

We further consider a Model 2, based on the accumulation rates of hemipelagic clastic material on the Ninety East Ridge at ODP Site 758 in the eastern BoB (Ali et al., 2021) (Fig. 3B). Site 758 is also potentially problematic in its direct use as a proxy for clastic erosional fluxes because it is located distally relative to the river mouth. Furthermore, hemipelagic sedimentation in this area may be influenced not only by the rate of sediment supply at the delta but also by sediment supply from the prograding Ayeyarwady (Irrawaddy) River in the past, as well as changes in oceanic circulation patterns in the evolving BoB during the Neogene. The northward drift of the Indian plate, coupled with progressive progradation of the Bengal delta, might be expected to drive increasing sediment supply to Site 758 through time independent of supply variability.

Finally, we consider a new sediment budget (Model 3) that assumes sediment flux in the BF mirrors the variability recorded in the western IF (Clift, 2006) (Fig. 3C). The similarity between the IF and collective regional budgets for SE Asia suggests a common climatically-controlled evolution of erosion rates during the Neogene (Clift, 2006). Erosion in the Ganga-Brahmaputra catchment might also be linked to the intensity of the South Asian monsoon, with stronger summer rains resulting in stronger erosion and more sedimentation in the submarine fans (Grujic et al., 2006; Gabet et al., 2008; Wulf et al., 2010). This seems reasonable because times of rapid sediment delivery to the IF correlate with times of rapid exhumation in the Greater Himalaya, which are also the dominant source of sediment to the BF (Clift et al., 2008). Because exhumation in the region is mostly driven by erosion, it is sensible that peak Early-Mid Miocene source exhumation would correlate with fast fan sedimentation, as predicted in Model 3. Sedimentation rates for the Nicobar Fan were estimated using a total fan volume of 1×10^6 km^3 and, in the absence of better constraints, the linear rates at IODP Site U1480 as a proxy for the total mass flux (McNeill et al., 2017a) (Fig. 3D).

This linkage between erosion and climate in the BF has been recently challenged using cosmogenic ^{10}Be records. Records document steady erosion rates since at least ~6.5 Ma in the Ganga-Brahmaputra suggest a lack of sensitivity to climate change (Lenard et al., 2020). These data are largely consistent with evidence from apatite fission track dating from the same cores that show no link between erosion rates and monsoon variability (Huyghe et al., 2020). If the occasional high erosion rates estimated by cosmogenic ^{10}Be are ignored, which contrast with the otherwise steady-state estimates, it remains possible to reconcile a net steady erosion rate to the BoB with changing climate if some degree of spatially variable sediment delivery is considered. For example, periodic erosion, storage and reworking within the foreland basin in response to changing climate conditions (Clift and Jonell, 2021b; Bhattacharjee et al., 2023) or changes in the relative contributions of mountain source catchments or materials, could at least partly account for this disparity.

4.4. Silicate weathering budgets

Silicate weathering budgets accounting for provenance evolution already exist for the Indus, Mekong and Pearl rivers systems over the last 16 m.y. (Clift and Jonell, 2021a), but no budget has previously been constructed for the BF. Provenance can be an important variable for consideration, especially if there is a large change in bedrock sources driving a shift in bulk major element compositions. We integrate each mass flux budget (Models 1–3) described above with the average compositions of BF sediment as sampled at the IODP drill sites for each time interval defined in the matching seismic data to estimate the CO_2 consumption induced by silicate weathering over significant time intervals. This compilation differs from earlier estimates by France-Lanord and Derry (1997) because our new compilation includes material sampled in the central BoB during IODP Expedition 354 (France-Lanord et al., 2016a), as well as the more distal Leg 116 (Cochran et al., 1989).

Although biogenic carbonate content in submarine fan sediments is generally low, corrections need to be made. $CaCO_3$ concentrations of 1–2% were measured at ODP Site 718 on the distal Bengal Fan (Shipboard Scientific Party, 1989) and 2–5% at Site U1451 on the mid Bengal Fan (France-Lanord et al., 2016b). The fan sediments at Site U1480 on the Nicobar Fan average 5–6% $CaCO_3$ content (McNeill et al., 2017c). Sediments from the Indus Fan at Sites U1456 and U1457 yielded values of 10–15% $CaCO_3$ (Pandey et al., 2016a; Pandey et al., 2016b). The Mekong-derived clastic sediments at Site U1433 average 4–6% carbonate (Li et al., 2015). At ODP Site 1148 in the northern South China Sea carbonate contents in the Neogene average at ~24% (Wang et al., 2000), but the bulk of sediment in this system resides in the Pearl River Basin, closer to the clastic sediment source and with less pelagic carbonate. We correct for the $CaCO_3$ contents with average values of 3% for the Bengal Fan, 12% for the Indus, 5.5% for the Nicobar, 5% for the Mekong and ~ 10% for the Pearl River.

Changes in the molar ratios of Mg/Al, Ca/Al, Na/Al and K/Al are used to calculate the moles of CO_2 sequestered during source bedrock breakdown (ΔCO_2)(France-Lanord and Derry, 1997). The elements Mg, Ca, Na and K are all preferentially removed relative to immobile Al through silicate chemical weathering. The mobility of Mg, Ca, Na and K is strongly grain-size dependent; smaller grains generally alter more rapidly because of their lower volume to surface area ratio and the vast majority of deep-sea sediment in the submarine fans is muddy silt (Prins et al., 2000; Weber et al., 2003). Sands are generally confined to volumetrically modest channels, and not much coarse-grained sediment was recovered at any of the drilling sites. By comparing compositions of altered sediment relative to fresh source bedrock, it is possible to determine how much CO_2 was removed per unit weight of weathered rock equivalent (ΔCO_2) (France-Lanord and Derry, 1997). If the total volume of sediment is constrained, then the total amount of CO_2 consumed can also be calculated for each time interval.

Estimates of the chemical weathering flux linked to the Nicobar Fan and BF were calculated using two possible bedrock end members: i) the average UCC composition (Rudnick and Gao, 2003) and ii) a compositional average of the Gangdese Batholith exposed across the suture zone in the northern part of the catchment. The average composition for the Gangdese Batholith was derived from 111 geochemical analyses of whole rocks sampled from the batholith within the Brahmaputra catchment compiled from the GEOROC database (Table 2). Previous work by Derry and France-Lanord (1997) utilized an average High Himalayan Crystalline (HHC) average rather than the UCC. Here, we suggest the UCC is somewhat more representative because HHC bedrock sampling in the past preferentially focused on leucogranite acquisition and less on the metamorphic bedrock that compositionally dominates the HHC (Hodges, 2000; Searle et al., 2006). This suggest the compositional average reconstructed using GEOROC is likely biased toward an average leucogranite composition. We argue that the BF catchment is large (1.72×10^6 km^3) and contains bedrock of generally typical continental composition, which implies an UCC average is more representative. Most sediment in the BF is derived from erosion of the Greater

Himalaya and Eastern Syntaxis (France-Lanord et al., 2006; Blum et al., 2018) that are dominated by variably metamorphosed and remelted fragments of the colliding continental Indian plate. Following the methodology of the IF system, we adjust the contribution of BF bedrock sources through time based on detrital zircon U—Pb geochronology data from the drill sites (Blum et al., 2018). This allows us to calculate the flux from the Gangdese Batholith relative to the more continental rocks in the rest of the catchment through time (Table 3 and Fig. 3E). We recognize that some of the sediment reaching the ocean is eroded from uplifted foreland basin sedimentary rocks that have already experienced weathering (Vögeli et al., 2017; Exnicios et al., 2022). However, work based from modern incision rates suggests that <15% of the sediment reaching the ocean is yielded from foreland bedrock (Lavé and Avouac, 2001) and therefore than the uncertainty introduced is not large.

5. Results

5.1. Silicate weathering

Chemical weathering in BF sediment can be estimated using the Chemical Index of Alteration (CIA)(Nesbitt et al., 1980). CIA values back to ~17 Ma show considerable scatter, with sediment values near fresh bedrock (<50) to almost 80 that are typical of intensely weathered sediment (Fig. 3F). A long-term five-point running average confirms little significant temporal trends in the data, except a modest rise in CIA after 7 Ma and a fall after 1 Ma. The sparse data coverage prior to 7 Ma may account for the lack of a clear trend at that time. It is important to note here that CIA trends merely show the degree of alteration of deposited sediment, rather than an estimate of the total amount of carbon sequestered during silicate weathering. The lack of coherent temporal trends in the BF is consistent with prior findings from the Mekong River (Clift and Jonell, 2021a). Within the Pearl and Indus Fans, CIA values broadly reduce through the Neogene.

5.2. Carbon dioxide consumption

Removing biogenic carbonate from the sediment is a critical step in assessing silicate chemical weathering and determining ΔCO_2 values. Ca is an important reactant in silicate chemical weathering processes but is naturally elevated in bulk sediment that contain carbonates. Since it is crucial to establish how much Ca is derived from silicates, all data compiled here are from sediment decarbonated prior to analysis. For example, recent work on BF sediment from Sites U1450 and U1451 by Tachambalath et al. (2023) shows the impact of calculating ΔCO_2 with poorly decarbonated sediments. ΔCO_2 values are substantially higher after only one round of decarbonation and higher yet again after more extensive treatment (Fig. 4A). Consequently, we consider all major element analyses from the BF that have not been successively decarbonated to be unreliable for estimating ΔCO_2. We therefore use the ~8 m.y. record from decarbonated sediments analyzed by Tachambalath et al. (2023) and then use the decarbonated results from France-Lanord and Derry (1997) from ODP Site 717 (Leg 116) to extend the record farther back in time to 16.1 Ma. Sediment from the Indus, Mekong and Pearl drainages were decarbonated prior to analysis (Wan et al., 2007; Liu et al., 2017; Zhou et al., 2021a) so can be considered reasonable materials for the calculation of ΔCO_2. But because all sediments, except those thoroughly decarbonated in the post-8 Ma BF by Tachambalath et al. (2023), may contain small amounts of remaining biogenic carbonate, it is reasonable to assume the resultant ΔCO_2 contributed by weathered Ca-rich silicates should be considered ΔCO_2 minima for each system.

Results from the Pearl River indicate slightly higher ΔCO_2 values yielded per kilogram of weathered rock than the BF, with the Indus and Mekong being both somewhat higher still (Fig. 4B). In part this may reflect the greater exposure of chemically reactive Ca- and Mg-rich mafic and ultramafic source rocks in the Indus headwaters compared to the Ganga-Brahmaputra system. Similar Ca- and Mg-rich primitive bedrock are also exposed in the Mekong headwaters (Huyan et al., 2023). Higher ΔCO_2 values may also in part reflect more intense weathering of

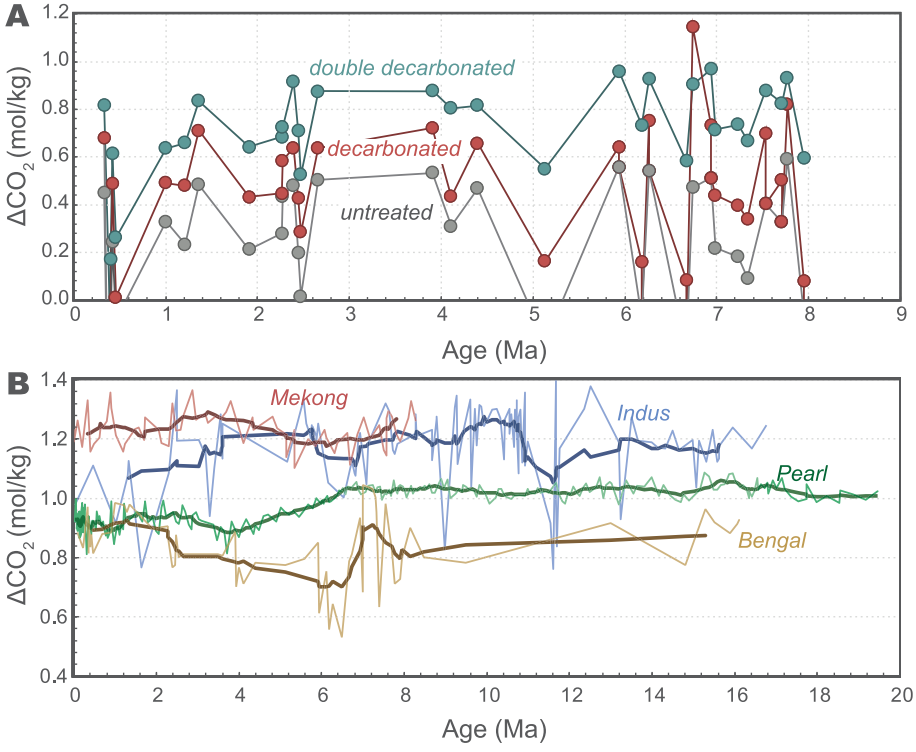

Fig. 4. A) Temporal evolution in ΔCO_2 from IODP Sites U1450 and U1451 (Tachambalath et al., 2023), showing the impact of decarbonation on the calculated values. B) Comparison of ΔCO_2 values for the four depocenters in this study. Fine lines show complete data variability and the thicker line shows the more representative 10 point running average.

sediment in the Indus catchment due to longer residence time onshore. This hypothesis and difference in source lithologies is broadly supported by use of a K/Si vs. Al/Si diagram, showing a steeper slope in the BF and the Mekong than in the offset Indus (Fig. 5)(Lupker et al., 2012b). Al/Si is a proxy for grain size because Al is contributed by clay-rich, fine-grained sediment whereas more Si is contributed from quartz-rich coarser sediment. K/Si is a proxy for weathering intensity because K is more water mobile than Si and fine-grained sediment tend to be more strongly weathered. Slopes on this diagram can be therefore indicative of the intensity of weathering of all sediment across grain sizes. The less intense weathering documented by BF and Mekong sediment could be the product of shorter onshore residence times controlled by the comparatively greater runoff increasing sediment transport, and therefore shorter residence, within these systems. A sub-population of low K/Si and Al/Si samples from the BF shows the occasional deposition of more strongly weathered material, if not consistently nor dominating the BF dataset.

There is still much disagreement concerning transport speed and duration of sediment residence time in floodplains. Modelling suggests that rivers with large flood plains might buffer sediment flux over tens to hundreds of kiloyears (Castelltort and Van Den Driessche, 2003). However, U-series dating of Ganga sediment suggests transit times spanning less than a year (Chabaux et al., 2012) to <20–25 k.y. (Granet et al., 2010) for fine grained sediments, while sandy sediment may take several 100's of k.y. (Granet et al., 2010). In the Indus fine-grained sediment is transported rapidly to the ocean after environment disturbance in the source areas, while sand appears to lag by ~5–7 k.y. (Clift and Giosan, 2014). However, final transport to the deep ocean may take 100 k.y. or longer (Clift and Jonell, 2021b; Bhattacharjee et al., 2023).

5.3. Organic carbon

Although many of the drilled sections do not penetrate deeper than the Lower Miocene, there is a common trend toward increasing OC near the tops of sections, correlating to sediment deposited after ~3 Ma (Fig. 2). Miocene OC values typically remain below 0.5%. The Miocene BF average OC is only 0.24%, contrasting with the previously reported average OC of 0.9% (France-Lanord and Derry, 1997). Although high OC levels have been found in sand-rich intervals in the BF (Lee et al., 2019), such sands remain volumetrically small compared to the total sediment mass. Therefore, even considering the sampling bias due to the difficulties in coring sand, sandy materials do not significantly affect the overall vertical/temporal OC distribution. OC values are similar in the Mekong (~0.5% in the Miocene) and much lower in Pearl River sites (~0.15% in the Miocene) (Fig. 2). This may reflect the comparatively more distal location of these drill sites (although they are not more distal than BF sites), which may contribute to decomposition of OC before deposition depending on how much OC was recycled onshore through the floodplains. It is well-documented that OC can oxidize during transit from source to sink, where its preservation is dependent on transit time and the degree of mineral protection around the OC prior to burial offshore (Repasch et al., 2021).

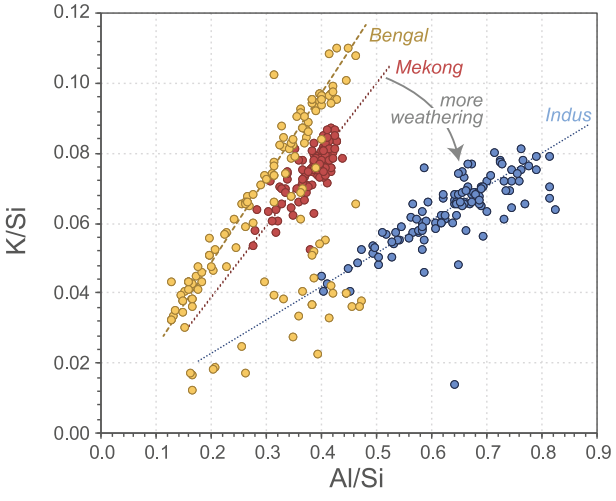

Fig. 5. Cross plot of K/Si versus Al/Si for samples from the Bengal, Indus, and Mekong fans showing that the former is less weathered than the latter two. After Lupker et al. (2012b). No SiO_2 data were available for the Pearl River/South China Sea samples.

When time-averaged OC values are integrated with rates of sediment delivery to each fan depocenter, it is possible to calculate total rates of OC burial according to each seismically resolved time interval (Table 1). Because IODP drilling only extended into Upper Miocene sediment in the IF (~10 Ma)(Routledge et al., 2020), we estimate the amount of OC stored before that time by applying Upper Miocene OC values to sediment delivery rates constrained for older intervals. An estimate is required if a regional Neogene carbon budget is to be constructed. Upper Miocene Pearl River and BF sediment OC concentrations are similar to Lower and Middle Miocene sediments and Upper Miocene IF sediment OC concentrations are not very variable (Fig. 2). The simplest assumption would be to assume a similar relationship for the IF as observed in the BF and Pearl River. In these more complete Miocene sections, OC values are stable through that period, which suggests that application of this estimate may offer a reasonable approximation of earlier OC burial rates.

5.4. Temporal evolution in fan carbon sequestration

Considering the BF (Fig. 6, Table 1), the CO_2 budget based on sedimentation Model 1 shows steady CO_2 consumption largely driven by silicate weathering that initiated in the early Miocene, increased in the late Miocene after 7 Ma, and with a marked increase in total OC burial rates in the Pliocene (Fig. 6A-B). Model 2 implies increases in both OC and weathering flux initiating in the middle Miocene (~13 Ma) after very low values prior to that time, followed much later by a Pliocene increase (Fig. 6C-D). It is noteworthy that in both Models 1 and 2, the CO_2 consumption by silicate weathering is greater than that attributed to OC burial, but that OC burial becomes a more important driver of the overall total carbon flux into the Pleistocene. Model 3 and application of the broadly comparable mass flux history in the IF to the BF results in high CO_2 consumption rates in the BF due to both OC burial and silicate weathering initiating even before the middle Miocene (Fig. 6F). This is the only model indicating significant levels of CO_2 consumption in the early Miocene and Oligocene. Similar to Models 1 and 2, Model 3 predicts that total CO_2 sequestration was dominated by silicate weathering processes but not OC burial. The Nicobar Fan, generally considered as an extension of the BF (Pickering et al., 2020), shows considerable variability after its initiation by ~11 Ma. Peak values occur in the early Pleistocene immediately prior to the cessation of sediment supply to this area (Fig. 6G-H).

Results for carbon burial from the BF can be compared with existing Asian fan data. OC burial in the Pearl River rises to a peak during the middle Miocene before decreasing in the Pliocene and increasing again in the Pleistocene. In the Pearl River, the contribution of OC burial to CO_2 consumption is relatively small (<10%), contributing only 31% to total carbon burial during the Pleistocene (Fig. 7A). Trends in the Pearl River follow a simple temporal evolution, reflecting the overall rate of clastic sedimentation to the region (Fig. 7B). Existing data from the Mekong cover initiation of the fan at its present location after ~8 Ma. Results indicate a modest contribution to total carbon burial with a greater proportion of OC burial (30–40%) contributing to total CO_2 consumption, rising to nearly ~60% in the Pliocene. There is a clear peak in carbon sequestration during the Pliocene in this area (Fig. 7D). OC burial in the IF also mirrors the history of clastic sedimentation; rising rapidly in the latter part of the early Miocene to reach a peak

Table 1
Carbon budget models for the depocenters considered in this study. Gray text indicates prediction based on extrapolating shallower data to deeper levels of the submarine fans.

	Mekong								
Age (Ma)	Delta CO_2 (mol/kg)	Carbonate adjussted total sediment flux ($*10^{11}$ kg/y)	Consumption CO_2 (Tmol/y)	Carbon reduction due to silicate weathering (Tmol/y)	Organic carbon (wt %)	Mass of Organic C buried (Mt/y)	Amount of Organic C buried (Tmol/y)	Total carbon burial (Tmol/y)	OC % of total carbon burial
1.80	0.822	0.651	0.054	0.054	0.562	0.385	0.032	0.086	37.4
2.58	0.827	0.679	0.056	0.056	0.432	0.309	0.026	0.082	31.4
3.60	0.883	0.679	0.060	0.060	1.627	1.163	0.097	0.157	61.8
5.33	0.830	0.443	0.037	0.037	0.703	0.328	0.027	0.064	42.6
7.25	0.791	0.442	0.035	0.035	0.409	0.190	0.016	0.051	31.2
10.50	0.845	0.346	0.029	0.029	1.038	0.378	0.031	0.061	51.8
10.90	0.853	0.346	0.030	0.030	1.038	0.378	0.031	0.061	51.6

	Pearl								
Age (Ma)	Delta CO_2 (mol/kg)	Carbonate adjussted total sediment flux ($*10^{11}$ kg/y)	Consumption CO_2 (Tmol/y)	Carbon reduction due to silicate weathering (Tmol/y)	Organic carbon (wt %)	Mass of Organic C buried (Mt/y)	Amount of Organic C buried (Tmol/y)	Total carbon burial (Tmol/y)	OC % of total carbon burial
1.80	0.890	0.123	0.011	0.011	0.471	0.064	0.005	0.016	32.8
2.58	0.911	0.123	0.011	0.011	0.193	0.026	0.002	0.013	16.4
3.60	0.894	0.123	0.011	0.011	0.115	0.016	0.001	0.012	10.6
5.33	0.886	0.123	0.011	0.011	0.106	0.014	0.001	0.012	10.0
7.25	0.973	0.080	0.008	0.008	0.106	0.009	0.001	0.009	9.1
10.50	0.996	0.080	0.008	0.008	0.164	0.015	0.001	0.009	13.2
10.90	0.982	0.080	0.008	0.008	0.100	0.009	0.001	0.009	8.6
11.63	0.990	0.080	0.008	0.008	0.060	0.005	0.000	0.008	5.3
13.00	0.994	0.205	0.020	0.020	0.122	0.028	0.002	0.023	10.2
13.82	1.002	0.205	0.021	0.021	0.035	0.008	0.001	0.021	3.1
14.80	0.985	0.205	0.020	0.020	0.135	0.031	0.003	0.023	11.3
15.50	0.998	0.205	0.020	0.020	0.088	0.020	0.002	0.022	7.5
15.97	1.025	0.205	0.021	0.021	0.083	0.019	0.002	0.023	7.0
17.00	1.009	0.205	0.021	0.021	0.092	0.021	0.002	0.022	7.8
18.00	0.992	0.205	0.020	0.020	0.112	0.025	0.002	0.022	9.4
19.50	0.978	0.112	0.011	0.011	0.095	0.012	0.001	0.012	8.2

	Indus								
Age (Ma)	Delta CO_2 (mol/kg)	Carbonate adjussted total sediment flux ($*10^{11}$ kg/y)	Consumption CO_2 (Tmol/y)	Carbon reduction due to silicate weathering (Tmol/y)	Organic carbon (wt %)	Mass of Organic C buried (Mt/y)	Amount of Organic C buried (Tmol/y)	Total carbon burial (Tmol/y)	OC % of total carbon burial
1.80	0.996	1.795	0.179	0.179	0.563	1.148	0.096	0.274	34.8
2.58	1.214	0.968	0.118	0.118	0.458	0.503	0.042	0.159	26.3
3.60	1.155	0.968	0.112	0.112	0.564	0.620	0.052	0.163	31.6
5.33	1.122	0.968	0.109	0.109	0.458	0.503	0.042	0.151	27.8
7.25	1.186	1.593	0.189	0.189	0.474	0.858	0.071	0.260	27.4
10.50	1.227	1.593	0.195	0.195	0.376	0.681	0.057	0.252	22.5
10.90	1.232	1.593	0.196	0.196	0.376	0.681	0.057	0.253	22.4
11.63	1.188	1.593	0.189	0.189	0.376	0.681	0.057	0.246	23.0
13.00	1.094	2.006	0.219	0.219	0.376	0.857	0.071	0.291	24.5
13.82	1.155	2.006	0.232	0.232	0.376	0.857	0.071	0.303	23.5
14.80	1.182	2.006	0.237	0.237	0.376	0.857	0.071	0.309	23.1
15.50	1.156	2.006	0.232	0.232	0.376	0.857	0.071	0.303	23.5
15.97	1.167	2.006	0.234	0.234	0.376	0.857	0.071	0.306	23.4
17.00	1.208	1.214	0.147	0.147	0.376	0.519	0.043	0.190	22.7
18.00	1.208	1.214	0.147	0.147	0.376	0.519	0.043	0.190	22.7
19.50	1.208	1.214	0.147	0.147	0.376	0.519	0.043	0.190	22.7
22.00	1.208	1.214	0.147	0.147	0.376	0.519	0.043	0.190	22.7
23.02	1.208	1.214	0.147	0.147	0.376	0.519	0.043	0.190	22.7
23.70	1.208	1.214	0.147	0.147	0.376	0.519	0.043	0.190	22.7
	1.208	0.774	0.094	0.094	0.376	0.331	0.028	0.121	22.7
	1.208	0.774	0.094	0.094	0.376	0.331	0.028	0.121	22.7

	Bengal (Model 1 budget)								
Age (Ma)	Delta CO_2 (mol/kg)	Carbonate adjussted total sediment flux ($*10^{11}$ kg/y)	Consumption CO_2 (Tmol/y)	Carbon reduction due to silicate weathering (Tmol/y)	Organic carbon (wt %)	Mass of Organic C buried (Mt/y)	Amount of Organic C	Total carbon burial (Tmol/y)	OC % of total carbon burial

(*continued on next page*)

Table 1 (*continued*)

	Bengal (Model 1 budget)								
Age (Ma)	Delta CO_2 (mol/kg)	Carbonate adjussted total sediment flux ($*10^{11}$ kg/y)	Consumption CO_2 (Tmol/y)	Carbon reduction due to silicate weathering (Tmol/y)	Organic carbon (wt %)	Mass of Organic C buried (Mt/y)	Amount of Organic C buried (Tmol/y)	Total carbon burial (Tmol/y)	OC % of total carbon burial
							buried (Tmol/y)		
1.80	0.873	6.936	0.606	0.606	0.659	4.713	0.392	0.998	39.3
2.58	0.924	4.895	0.453	0.453	0.334	1.686	0.140	0.593	23.7
3.60	0.905	4.895	0.443	0.443	0.257	1.295	0.108	0.551	19.6
5.33	0.804	4.895	0.394	0.394	0.348	1.753	0.146	0.539	27.1
7.25	0.807	3.062	0.247	0.247	0.421	1.329	0.111	0.358	30.9
10.50	0.786	3.062	0.241	0.241	0.271	0.854	0.071	0.312	22.8
10.90	0.786	3.062	0.241	0.241	0.268	0.844	0.070	0.311	22.6
11.63	0.786	3.062	0.241	0.241	0.267	0.842	0.070	0.311	22.5
13.00	0.916	3.062	0.280	0.280	0.323	1.021	0.085	0.365	23.3
13.82	0.916	3.062	0.280	0.280	0.252	0.795	0.066	0.347	19.1
14.80	0.916	3.062	0.280	0.280	0.227	0.717	0.060	0.340	17.5
15.50	0.941	3.062	0.288	0.288	0.223	0.705	0.059	0.347	16.9
15.97	0.881	3.062	0.270	0.270	0.299	0.943	0.078	0.348	22.5
17.00	0.914	3.062	0.280	0.280	0.289	0.913	0.076	0.356	21.3
18.00	0.914	3.062	0.280	0.280	0.100	0.316	0.026	0.306	8.6
19.50	0.914	3.062	0.280	0.280	0.100	0.316	0.026	0.306	8.6
22.00	0.914	3.062	0.280	0.280	0.150	0.474	0.039	0.319	12.3
23.02	0.914	3.062	0.280	0.280	0.100	0.316	0.026	0.306	8.6
23.70	0.914	1.302	0.119	0.119	0.100	0.134	0.011	0.130	8.6

	Bengal (Model 2 budget)								
Age (Ma)	Delta CO_2 (mol/kg)	Carbonate adjussted total sediment flux ($*10^{11}$ kg/y)	Consumption CO_2 (Tmol/y)	Carbon reduction due to silicate weathering (Tmol/y)	Organic carbon (wt %)	Mass of Organic C buried (Mt/y)	Amount of Organic C buried (Tmol/y)	Total carbon burial (Tmol/y)	OC % of total carbon burial
1.80	0.873	8.702	0.760	0.760	0.659	5.913	0.492	1.252	39.3
2.58	0.924	9.090	0.840	0.840	0.334	3.130	0.261	1.101	23.7
3.60	0.905	7.099	0.642	0.642	0.257	1.878	0.156	0.799	19.6
5.33	0.804	5.782	0.465	0.465	0.348	2.071	0.172	0.637	27.1
7.25	0.807	4.959	0.400	0.400	0.421	2.152	0.179	0.580	30.9
10.50	0.786	3.801	0.299	0.299	0.271	1.061	0.088	0.387	22.8
10.90	0.786	3.801	0.299	0.299	0.268	1.048	0.087	0.386	22.6
11.63	0.786	3.801	0.299	0.299	0.267	1.045	0.087	0.386	22.5
13.00	0.916	1.066	0.098	0.098	0.323	0.355	0.030	0.127	23.3
13.82	0.916	1.280	0.117	0.117	0.252	0.332	0.028	0.145	19.1
14.80	0.916	0.677	0.062	0.062	0.227	0.158	0.013	0.075	17.5
15.50	0.941	0.677	0.064	0.064	0.223	0.156	0.013	0.077	16.9
15.97	0.881	1.200	0.106	0.106	0.299	0.369	0.031	0.137	22.5
17.00	0.914	1.088	0.100	0.100	0.289	0.324	0.027	0.127	21.3
18.00	0.914	1.088	0.100	0.100	0.100	0.112	0.009	0.109	8.6
19.50	0.914	1.286	0.118	0.118	0.100	0.133	0.011	0.129	8.6
22.00	0.914	1.511	0.138	0.138	0.150	0.234	0.019	0.158	12.3
23.02	0.914	1.131	0.103	0.103	0.100	0.117	0.010	0.113	8.6
23.70	0.914	1.167	0.107	0.107	0.100	0.120	0.010	0.117	8.6

	Bengal (Model 3 budget)								
Age (Ma)	Delta CO_2 (mol/kg)	Carbonate adjussted total sediment flux ($*10^{11}$ kg/y)	Consumption CO_2 (Tmol/y)	Carbon reduction due to silicate weathering (Tmol/y)	Organic carbon (wt %)	Mass of Organic C buried (Mt/y)	Amount of Organic C buried (Tmol/y)	Total carbon burial (Tmol/y)	OC % of total carbon burial
1.80	0.873	4.797	0.419	0.419	0.659	3.260	0.271	0.690	39.3
2.58	0.924	2.587	0.239	0.239	0.334	0.891	0.074	0.313	23.7
3.60	0.905	2.587	0.234	0.234	0.257	0.684	0.057	0.291	19.6
5.33	0.804	2.587	0.208	0.208	0.348	0.927	0.077	0.285	27.1
7.25	0.807	4.256	0.344	0.344	0.421	1.847	0.154	0.497	30.9
10.50	0.786	4.256	0.335	0.335	0.271	1.188	0.099	0.434	22.8
10.90	0.786	4.256	0.335	0.335	0.268	1.174	0.098	0.432	22.6
11.63	0.786	4.256	0.335	0.335	0.267	1.170	0.097	0.432	22.5
13.00	0.916	5.361	0.491	0.491	0.323	1.787	0.149	0.640	23.3
13.82	0.916	5.361	0.491	0.491	0.252	1.393	0.116	0.607	19.1
14.80	0.916	5.361	0.491	0.491	0.227	1.255	0.104	0.596	17.5
15.50	0.941	5.361	0.504	0.504	0.223	1.234	0.103	0.607	16.9
15.97	0.881	5.361	0.472	0.472	0.299	1.650	0.137	0.610	22.5

(*continued on next page*)

Table 1 (*continued*)

	Bengal (Model 3 budget)								
Age (Ma)	Delta CO_2 (mol/kg)	Carbonate adjussted total sediment flux (*10^{11} kg/y)	Consumption CO_2 (Tmol/y)	Carbon reduction due to silicate weathering (Tmol/y)	Organic carbon (wt %)	Mass of Organic C buried (Mt/y)	Amount of Organic C buried (Tmol/y)	Total carbon burial (Tmol/y)	OC % of total carbon burial
17.00	0.914	3.245	0.297	0.297	0.289	0.967	0.081	0.377	21.3
18.00	0.914	3.245	0.297	0.297	0.100	0.335	0.028	0.325	8.6
19.50	0.914	3.245	0.297	0.297	0.100	0.335	0.028	0.325	8.6
22.00	0.914	3.245	0.297	0.297	0.150	0.502	0.042	0.338	12.3
23.02	0.914	3.245	0.297	0.297	0.100	0.335	0.028	0.325	8.6
23.70	0.914	3.245	0.297	0.297	0.100	0.335	0.028	0.325	8.6

	Nicobar								
Age (Ma)	Delta CO_2 (mol/kg)	Carbonate adjussted total sediment flux (*10^{11} kg/y)	Consumption CO_2 (Tmol/y)	Carbon reduction due to silicate weathering (Tmol/y)	Organic carbon (wt %)	Mass of Organic C buried (Mt/y)	Amount of Organic C buried (Tmol/y)	Total carbon burial (Tmol/y)	OC % of total carbon burial
1.80	0.873	0.141	0.012	0.012	0.378	0.056	0.005	0.017	27.6
2.58	0.924	2.734	0.253	0.253	0.523	1.513	0.126	0.379	33.3
3.60	0.905	1.187	0.107	0.107	0.369	0.464	0.039	0.146	26.5
5.33	0.804	0.618	0.050	0.050	0.286	0.187	0.016	0.065	23.9
7.25	0.807	1.727	0.139	0.139	0.369	0.674	0.056	0.196	28.7
10.50	0.786	1.129	0.089	0.089	0.402	0.480	0.040	0.129	31.1
10.90	0.786	1.129	0.089	0.089	0.402	0.480	0.040	0.129	31.1

Table 2
Composition of sources used in the calculation of CO2 consumption. UCC is from Rudnick and Gao (2003). Gangdese Batholith average is from GEOROC database. Upper Indus is from sediment of the upper reaches from Alizai et al. (2011).

SiO_2 (wt%)	Al_2O_3 (wt%)	Fe_2O_3 (wt%)	CaO (wt%)	MgO (wt%)	Na_2O (wt%)	K_2O (wt %)	P_2O_5 (wt%)
Upper Continental Crust - Rudnick and Gao							
66.62	15.40	5.04	3.59	2.48	3.27	2.80	0.15
Gangdese Batholith							
57.26	16.23	7.12	3.39	5.84	3.53	2.01	0.25
Upper Indus							
69.74	11.11	4.04	2.20	5.34	2.05	2.11	0.12

during the middle Miocene (Fig. 7E). A general decline in burial rates is documented up to the Pliocene, followed by an increase into the Pleistocene. OC burial represents around 25–30% of the total carbon budget calculated for the IF, with a maximum of 34% in the Pleistocene (Fig. 7F).

When the BF (Model 2) and Nicobar systems budgets are combined to obtain a regional budget for the entire BoB, a broad long-term increase in OC burial emerges (Fig. 7G). OC burial rates rose at the end of the middle Miocene, and especially sharply in the Pliocene. OC burial accounts for ~10% of the total budget in the early Miocene, rising to ~20% in the middle-late Miocene, and then increasing again to reach a maximum of ~39% in the Pleistocene. Contribution of OC burial to the total flux increased at ~13 Ma and after ~4 Ma (Fig. 7H).

A regional carbon flux budget through time can be made from the combined OC burial and silicate weathering budgets from all deep-sea depocenters (Fig. 8 and Table 4). We use the results from sediment flux Model 2 for the BF as an example because it has the highest temporal resolution and has been recently employed in other work (Ali et al., 2021; Song et al., 2023). Burial of OC in Asian fans began to increase by the early Miocene (Fig. 8A), with a particularly noticeable increase after 11.6 Ma and again after 5 Ma. Prior to ~13 Ma, OC burial in the IF was the most important carbon sink, with OC burial in this fan peaking at 83% of the total OC by 15.5 Ma. Nonetheless, OC burial in the BF subsequently increased such that the BF accounted for 60% of the regional total by 11.6 Ma, and even further contributed as much as 78% of the regional total OC flux after 3.6 Ma.

Trends in total CO_2 consumption linked to silicate chemical weathering, as recorded by Asian fans, are somewhat different (Fig. 8B). The IF emerges as the single largest early Neogene consumer of CO_2, with consumption peaking at 66% of the total Asian fan flux in the middle Miocene (~14.8 Ma). After ~13 Ma, the proportion consumed by silicate weathering in the BF, as well as by OC burial, increases. Subsequently, the BF independently accounts for 65% of the total consumption by silicate weathering in the early Pleistocene. If considered with the Nicobar Fan, this jumps to nearly 85% of the Asian fan total. Through the Neogene, total carbon sequestration rates from Asian fans show a modest increase after 17 Ma, with especially marked increases at ~13 and ~ 5 Ma (Fig. 8C).

6. Discussion

6.1. History of organic carbon burial

Most drill sites compiled here show increasing OC concentrations upsection (Fig. 2), which may reflect increased OC delivery from source river systems and/or better preservation of OC toward the present day. The measured OC concentrations do not account for the fraction of sediment OC that is lost through microbial processing, which is termed OC mineralization (Sobek et al., 2009; Gudasz et al., 2010). Both faster OC transport or increased clastic sedimentation could result in more efficient OC burial, leading to reduced OC oxidation and therefore better preservation of OC in the sedimentary record. This could explain the trend recorded in the BF after ~3 Ma. While it is argued that OC has been efficiently buried in the BF in the recent past (Galy et al., 2007), this may not have been the case prior to the Pleistocene when sedimentation rates in the BF were lower. Slower burial could have increased oxidation potential of OC on the seafloor and greater OC mineralization, lending to poorer preservation of OC in the past (Rothman and Forney, 2007). Broadly, there is a clear trend across all records with increasing rate of OC burial through time, especially at the start of the late Miocene and the Pliocene. This would be consistent with the idea that OC burial might be a control over global CO_2 budgets at those times (Shackleton, 1987).

The growing dominance of the BF through the Neogene on the regional OC budget is not surprising given its great volume (Fig. 8A).

Table 3
Compilation of BF sediment compositions used to calculate the chemical weathering flux for that depocenter. Data from Sites U1450 and U1451 are from Tachambalath et al. (2023). Data from Site 717 is from France-Lanord and Derry (1997).

Hole	Sample	Age (Ma)	Percentage Gangdese	SiO_2 (wt%)	Al_2O_3 (wt%)	$Ti0_2$ (wt%)	Fe_2O_3 (wt%)	MgO (wt%)	CaO (wt%)	Na_2O (wt%)	K_2O (wt%)	MnO (wt%)	P_2O_5 (wt%)
354-U1451A-	6H-1, 72–76	0.33	25	64.28	15.61	0.69	5.56	2.71	4.15	3.33	2.60	0.11	0.17
354-U1450A-	7F-1, 47–52	0.35	25	64.28	15.61	0.69	5.56	2.71	4.15	3.33	2.60	0.11	0.17
354-U1451A-	9H-1, 68–73	0.40	25	64.28	15.61	0.69	5.56	2.71	4.15	3.33	2.60	0.11	0.17
354-U1451A-	10F-3, 28–33	0.42	25	64.28	15.61	0.69	5.56	2.71	4.15	3.33	2.60	0.11	0.17
354-U1451A-	11F-3, 55–60	0.46	25	64.28	15.61	0.69	5.56	2.71	4.15	3.33	2.60	0.11	0.17
354-U1450A-	28F-1, 84–89	1.00	25	64.28	15.61	0.69	5.56	2.71	4.15	3.33	2.60	0.11	0.17
354-U1451A-	16F-2, 91–96	1.21	25	64.28	15.61	0.69	5.56	2.71	4.15	3.33	2.60	0.11	0.17
354-U1450A-	38F-2, 100–105	1.36	25	64.28	15.61	0.69	5.56	2.71	4.15	3.33	2.60	0.11	0.17
354-U1450A-	54F-2, 54–59	1.91	25	64.28	15.61	0.69	5.56	2.71	4.15	3.33	2.60	0.11	0.17
354-U1450A-	74F-2, 54–56	2.27	30	63.81	15.65	0.70	5.66	2.75	4.27	3.35	2.56	0.11	0.18
354-U1450A-	74F-2, 52–54	2.27	30	63.81	15.65	0.70	5.66	2.75	4.27	3.35	2.56	0.11	0.18
354-U1451A-	22H-1, 41–46	2.39	30	63.81	15.65	0.70	5.66	2.75	4.27	3.35	2.56	0.11	0.18
354-U1451A-	23H-5, 16–21	2.44	30	63.81	15.65	0.70	5.66	2.75	4.27	3.35	2.56	0.11	0.18
354-U1451A-	24H-2, 29–34	2.47	30	63.81	15.65	0.70	5.66	2.75	4.27	3.35	2.56	0.11	0.18
354-U1450A-	94F-1, 50–55	2.66	30	63.81	15.65	0.70	5.66	2.75	4.27	3.35	2.56	0.11	0.18
354-U1450A-	110F-1, 79–84	3.50	22	64.56	15.58	0.68	5.50	2.68	4.09	3.33	2.63	0.11	0.17
354-U1450A-	119F-1, 73–79	3.90	22	64.56	15.58	0.68	5.50	2.68	4.09	3.33	2.63	0.11	0.17
354-U1450A-	122×-1108–112	4.10	10	65.68	15.48	0.66	5.25	2.57	3.82	3.30	2.72	0.10	0.16
354-U1450A-	126F-1, 66–70	4.40	10	65.68	15.48	0.66	5.25	2.57	3.82	3.30	2.72	0.10	0.16
354-U1451A-	27H-2, 26–31	5.13	10	65.68	15.48	0.66	5.25	2.57	3.82	3.30	2.72	0.10	0.16
354-U1451A-	30H-5, 38–43	5.94	10	65.68	15.48	0.66	5.25	2.57	3.82	3.30	2.72	0.10	0.16
354-U1451A-	33F-4, 12–17	6.18	10	65.68	15.48	0.66	5.25	2.57	3.82	3.30	2.72	0.10	0.16
354-U1451A-	35F-1, 27–32	6.27	10	65.68	15.48	0.66	5.25	2.57	3.82	3.30	2.72	0.10	0.16
354-U1451A-	41F-1, 70–75	6.67	10	65.68	15.48	0.66	5.25	2.57	3.82	3.30	2.72	0.10	0.16
354-U1450A-	136×-2, 42–46	6.74	10	65.68	15.48	0.66	5.25	2.57	3.82	3.30	2.72	0.10	0.16
354-U1451A-	45F-1, 90–92	6.94	10	65.68	15.48	0.66	5.25	2.57	3.82	3.30	2.72	0.10	0.16
354-U1450B-	12R-3, 46–48	6.99	10	65.68	15.48	0.66	5.25	2.57	3.82	3.30	2.72	0.10	0.16
354-U1450B-	16R-3, 110–115	7.23	10	65.68	15.48	0.66	5.25	2.57	3.82	3.30	2.72	0.10	0.16
354-U1450B-	18R-1, 55–57	7.34	10	65.68	15.48	0.66	5.25	2.57	3.82	3.30	2.72	0.10	0.16
354-U1451A-	54F-1104–109	7.54	10	65.68	15.48	0.66	5.25	2.57	3.82	3.30	2.72	0.10	0.16
354-U1451A-	56F-3, 132–137	7.71	10	65.68	15.48	0.66	5.25	2.57	3.82	3.30	2.72	0.10	0.16
354-U1450B-	21R-2, 19–21	7.77	10	65.68	15.48	0.66	5.25	2.57	3.82	3.30	2.72	0.10	0.16
354-U1451A-	60F-2, 80–84	7.95	10	65.68	15.48	0.66	5.25	2.57	3.82	3.30	2.72	0.10	0.16
116–717-		0.09	25	64.28	15.61	0.69	5.56	2.71	4.15	3.33	2.60	0.11	0.17
116–717-		0.23	25	64.28	15.61	0.69	5.56	2.71	4.15	3.33	2.60	0.11	0.17
116–717-		0.35	25	64.28	15.61	0.69	5.56	2.71	4.15	3.33	2.60	0.11	0.17
116–717-		0.40	25	64.28	15.61	0.69	5.56	2.71	4.15	3.33	2.60	0.11	0.17
116–717-		0.70	25	64.28	15.61	0.69	5.56	2.71	4.15	3.33	2.60	0.11	0.17
116–717-		0.90	25	64.28	15.61	0.69	5.56	2.71	4.15	3.33	2.60	0.11	0.17

(*continued on next page*)

Table 3 (*continued*)

Hole	Sample	Age (Ma)	Percentage Gangdese	SiO_2 (wt%)	AI_2O_3 (wt%)	$Ti0_2$ (wt%)	Fe_2O_3 (wt%)	MgO (wt%)	CaO (wt%)	Na_2O (wt%)	K_2O (wt%)	MnO (wt%)	P_2O_5 (wt%)
116–717-		1.29	25	64.28	15.61	0.69	5.56	2.71	4.15	3.33	2.60	0.11	0.17
116–717-		2.55	30	63.81	15.65	0.70	5.66	2.75	4.27	3.35	2.56	0.11	0.18
116–717-		3.60	22	64.56	15.58	0.68	5.50	2.68	4.09	3.33	2.63	0.11	0.17
116–717-		3.94	22	64.56	15.58	0.68	5.50	2.68	4.09	3.33	2.63	0.11	0.17
116–717-		4.01	10	65.68	15.48	0.66	5.25	2.57	3.82	3.30	2.72	0.10	0.16
116–717-		5.57	10	65.68	15.48	0.66	5.25	2.57	3.82	3.30	2.72	0.10	0.16
116–717-		5.92	10	65.68	15.48	0.66	5.25	2.57	3.82	3.30	2.72	0.10	0.16
116–717-		6.11	10	65.68	15.48	0.66	5.25	2.57	3.82	3.30	2.72	0.10	0.16
116–717-		6.50	10	65.68	15.48	0.66	5.25	2.57	3.82	3.30	2.72	0.10	0.16
116–717-		7.00	10	65.68	15.48	0.66	5.25	2.57	3.82	3.30	2.72	0.10	0.16
116–717-		7.00	10	65.68	15.48	0.66	5.25	2.57	3.82	3.30	2.72	0.10	0.16
116–717-		7.30	10	65.68	15.48	0.66	5.25	2.57	3.82	3.30	2.72	0.10	0.16
116–717-		7.40	10	65.68	15.48	0.66	5.25	2.57	3.82	3.30	2.72	0.10	0.16
116–717-		7.90	10	65.68	15.48	0.66	5.25	2.57	3.82	3.30	2.72	0.10	0.16
116–717-		8.15	10	65.68	15.48	0.66	5.25	2.57	3.82	3.30	2.72	0.10	0.16
116–717-		8.48	10	65.68	15.48	0.66	5.25	2.57	3.82	3.30	2.72	0.10	0.16
116–717-		9.50	10	65.68	15.48	0.66	5.25	2.57	3.82	3.30	2.72	0.10	0.16
116–717-		13.00	10	65.68	15.48	0.66	5.25	2.57	3.82	3.30	2.72	0.10	0.16
116–717-		14.80	10	65.68	15.48	0.66	5.25	2.57	3.82	3.30	2.72	0.10	0.16
116–717-		15.30	10	65.68	15.48	0.66	5.25	2.57	3.82	3.30	2.72	0.10	0.16
116–717-		15.50	10	65.68	15.48	0.66	5.25	2.57	3.82	3.30	2.72	0.10	0.16
116–717-		15.89	10	65.68	15.48	0.66	5.25	2.57	3.82	3.30	2.72	0.10	0.16
116–717-		16.06	10	65.68	15.48	0.66	5.25	2.57	3.82	3.30	2.72	0.10	0.16
116–717-		16.10	10	65.68	15.48	0.66	5.25	2.57	3.82	3.30	2.72	0.10	0.16

Yet, it is also clear that, regardless of which sedimentation model is employed, the contribution of OC burial to the total carbon flux is often subsidiary to the consumption led by silicate weathering. OC burial accounts for only 16–22% of the total in the early Miocene, 21–24% in the middle Miocene, and 25–30% in the late Miocene before peaking to as much as 38% in the Pleistocene (Table 5). It is likely that some of the buried OC in all fans is recycled petrogenic OC, which suggests that estimates made here regarding OC burial consumption may be overestimated. In the BF sedimentation model with the highest Pliocene-Pleistocene sedimentation rate (Model 2), the total OC burial contribution to the total carbon flux reached as much as 38%, which is similar in magnitude to the other models considered. Comparison of three separate BF sedimentation models in this study emphasizes the importance of constraining a representative and reliable sedimentation budget because they remain critical for reconstructing silicate chemical weathering and OC burial fluxes. Given the observed variability in OC content across Asian fans (Fig. 2) and that the weathering intensity through the Neogene is relatively limited (Fig. 4), the total carbon flux is principally governed by the rate of sediment delivery to Asian fan depocenters, as also recognized by Jin et al. (2023).

6.2. Regional differences

The Model 2 budget for the Nicobar and BF (Fig. 7G and H) predicts that CO_2 drawdown by silicate chemical weathering increased during the latter part of the middle Miocene and again in the Pliocene. Prior to the late Miocene, more CO_2 was removed by the IF relative to the BF (Fig. 8C). Despite its smaller catchment size, the more reactive primitive bedrock exposed within the Indus catchment (Fig. 4B) helped to enhance the greater chemical weathering flux before ~11 Ma; although this flux estimate is mostly a function of rapid sediment deposition offshore. During the middle Miocene, ~65–75% of the total CO_2 consumption in South and SE Asia appears driven by the Indus. In contrast, the Pearl River peaks at only ~7% of the total in the early Miocene, with the Mekong accounting for as much as 12% in the mid-late Pliocene. When the Nicobar Fan was active, it contributed a significant amount to the total carbon budget, reaching ~22% of the total flux in the early Pleistocene (Fig. 8C, Table 4).

The Pearl and the Indus depocenters show highest contributions to the total carbon flux during the middle Miocene when sediment fluxes were at their maxima. A later increase in Pearl and Indus OC burial occurred in the Pleistocene when sediment fluxes increased again (Fig. 7A and E). If the Model 2 budget is assumed for the BF, then this implies a quite different evolution in that drainage basin, with a relatively modest impact on carbon flux in the middle Miocene and the greatest impact on the total carbon budget occurring only after ~11.6 Ma (Fig. 8C). In this model it is noteworthy that the total carbon consumption assigned to the Nicobar Fan and BF has increased gradually since the middle Miocene, with a maximum in the Early Pleistocene (Fig. 7H).

6.3. Comparison with modern fluxes

Reconstructed CO_2 consumption rates driven by silicate weathering and presented here are high when compared to values derived from modern dissolved load geochemistry. Ganga-Brahmaputra silicate weathering was estimated to result in a drawdown rate of as low as 0.064 Tmol/yr CO_2 by Galy and France-Lanord (1999) and up to 0.31 Tmol/y by Suchet et al. (2003). Alternately, 0.47 Tmol/y is estimated from the Ganga (Gaillardet et al., 1999) and 0.27 Tmol/y for the Brahmaputra (Singh et al., 2005), separately. The latter estimates are lower but generally most comparable to our late Pleistocene averages of 0.62 Tmol/yr (Model 1), 0.78 Tmol/yr (Model 2) and 0.43 Tmol/yr (Model 3) yielded from the BF. In contrast, silicate-related CO_2 drawdown estimated from decadal-averaged river chemistry from the Mekong yields values of 0.15 Tmol/yr to 0.19 Tmol/yr from the modern river (Gaillardet et al., 1999; Suchet et al., 2003; Li et al., 2014) compared to 0.056 Tmol/yr yielded in this study. Analysis of Indus River water near the river mouth (February 1992; Pande et al. (1994)) indicates that silicate-related CO_2 consumption rate is 0.054 Tmol/y (Gaillardet et al., 1999), compared to 0.20 Tmol/y estimated here. The largest western part of the Pearl River (Xijiang tributary) indicates silicate-related CO_2 consumption from 0.024 to 0.054 Tmol/y (Gaillardet et al., 1999; Xu and Liu, 2010), while we estimate only 0.012 Tmol/y.

In general, the Himalaya-draining rivers (Indus and Ganga-Brahmaputra) appear to show the greatest difference between long-term averages derived from the deep-sea sediment record and measured from near-modern rivers. Some of this apparent difference may be reconciled simply due to our analysis of the integrated systems at their final depocenters rather than from onshore rivers and subaerial deltas, and by long-term averaging over intervals when weathering rates changed significantly. A long-term Pleistocene-Holocene estimate of

Table 4
Summary carbon/CO_2 budget showing the total flux for each of the submarine fans through time broken down in organic carbon, silicate weathering related, total and the percentage of the total regional budget.

	Organic carbon					Silicate weathering				
Age (Ma)	Mekong (Tmol/y)	Pearl (Tmol/y)	Indus (Tmol/y)	Bengal (Tmol/y)	Nicobar (Tmol/y)	Mekong (Tmol/y)	Pearl (Tmol/y)	Indus (Tmol/y)	Bengal (Tmol/y)	Nicobar (Tmol/y)
1.80	0.0320	0.0053	0.0956	0.4923	0.0047	0.0563	0.0109	0.1787	0.7599	0.0123
2.58	0.0257	0.0022	0.0419	0.2606	0.1260	0.0591	0.0112	0.1175	0.8404	0.2527
3.60	0.0969	0.0013	0.0516	0.1564	0.0386	0.0631	0.0110	0.1118	0.6421	0.1073
5.33	0.0273	0.0012	0.0419	0.1725	0.0156	0.0387	0.0109	0.1086	0.4649	0.0497
7.25	0.0159	0.0008	0.0714	0.1792	0.0561	0.0369	0.0078	0.1889	0.4004	0.1395
10.50	0.0315	0.0012	0.0567	0.0883	0.0400	0.0308	0.0080	0.1954	0.2989	0.0887
10.90	0.0315	0.0007	0.0567	0.0873	0.0400	0.0311	0.0079	0.1963	0.2989	0.0887
11.63		0.0004	0.0567	0.0870	0.0000		0.0079	0.1892	0.2989	0.0000
13.00		0.0023	0.0714	0.0296	0.0000		0.0204	0.2195	0.0976	0.0000
13.82		0.0007	0.0714	0.0277	0.0000		0.0206	0.2317	0.1172	0.0000
14.80		0.0026	0.0714	0.0132	0.0000		0.0202	0.2372	0.0620	0.0000
15.50		0.0017	0.0714	0.0130	0.0000		0.0205	0.2320	0.0637	0.0000
15.97		0.0016	0.0714	0.0308	0.0000		0.0210	0.2342	0.1058	0.0000
17.00		0.0017	0.0432	0.0270	0.0000		0.0207	0.1467	0.0995	0.0000
18.00		0.0021	0.0432	0.0093	0.0000		0.0204	0.1467	0.0995	0.0000
19.50		0.0010	0.0432	0.0110	0.0000		0.0110	0.1467	0.1176	0.0000
22.00		0.0010	0.0432	0.0195			0.0113	0.1467	0.1382	0.0020
23.02		0.0010	0.0432	0.0097			0.0113	0.1467	0.1034	0.0020
23.70		0.0010	0.0432	0.0100			0.0113	0.1467	0.1067	0.0020
27.82			0.0275	0.0000				0.0935		
28.40			0.0275	0.0000				0.0935		

	Total					Relative contribution				
Age (Ma)	Mekong (Tmol/y)	Pearl (Tmol/y)	Indus (Tmol/y)	Bengal (Tmol/y)	Nicobar (Tmol/y)	Indus %	Bengal %	Nicobar %	Pearl %	Mekong %
1.80	0.0884	0.0175	0.2987	1.2757	0.0177	17.6	75.1	1.0	1.0	5.2
2.58	0.0849	0.0146	0.1754	1.1270	0.3935	9.8	62.8	21.9	0.8	4.7
3.60	0.1600	0.0135	0.1787	0.8184	0.1522	13.5	61.9	11.5	1.0	12.1
5.33	0.0660	0.0133	0.1653	0.6517	0.0681	17.1	67.6	7.1	1.4	6.8
7.25	0.0527	0.0095	0.2860	0.5919	0.2037	25.0	51.7	17.8	0.8	4.6
10.50	0.0623	0.0101	0.2788	0.3964	0.1339	31.6	45.0	15.2	1.1	7.1
10.90	0.0626	0.0095	0.2797	0.3954	0.1339	31.7	44.9	15.2	1.1	7.1
11.63	0.0000	0.0093	0.2717	0.3951	0.0000	40.2	58.4	0.0	1.4	0.0
13.00	0.0000	0.0250	0.3208	0.1302	0.0000	67.4	27.4	0.0	5.2	0.0
13.82	0.0000	0.0235	0.3347	0.1485	0.0000	66.1	29.3	0.0	4.6	0.0
14.80	0.0000	0.0250	0.3409	0.0771	0.0000	76.9	17.4	0.0	5.7	0.0
15.50	0.0000	0.0244	0.3350	0.0787	0.0000	76.5	18.0	0.0	5.6	0.0
15.97	0.0000	0.0250	0.3375	0.1398	0.0000	67.2	27.8	0.0	5.0	0.0
17.00	0.0000	0.0248	0.2099	0.1296	0.0000	57.6	35.6	0.0	6.8	0.0
18.00	0.0000	0.0247	0.2099	0.1119	0.0000	60.6	32.3	0.0	7.1	0.0
19.50	0.0000	0.0132	0.2099	0.1322	0.0000	59.1	37.2	0.0	3.7	0.0
22.00	0.0000	0.0136	0.2099	0.1619	0.0020	54.2	41.8	0.5	3.5	0.0
23.02	0.0000	0.0136	0.2099	0.1163	0.0020	61.4	34.0	0.6	4.0	0.0
23.70	0.0000	0.0136	0.2099	0.1200	0.0020	60.8	34.7	0.6	3.9	0.0
27.82	0.0000	0.0000	0.1338	0.0000	0.0000	100.0	0.0	0.0	0.0	0.0
28.40	0.0000	0.0000	0.1338	0.0000	0.0000	100.0	0.0	0.0	0.0	0.0

~900–1400 Mt./y sediment flux from the postglacial Indus delta (Clift and Jonell, 2021b) compares to pre-industrial Indus River fluxes of ~250–300 Mt./y (Milliman and Syvitski, 1992) to as high as 475 Mt./y (Holeman, 1968; Meybeck, 1976; Summerfield and Hulton, 1994). The difference in weathering flux estimates could be due to retention of sediment onshore at the delta and shelf during sea level high stands, although such a process would be averaged out as the material is redeposited into the deep IF during sea level low stands. IF sediment fluxes reached their highest average values over the Pleistocene (~200 Mt./y) and middle Miocene (~250 Mt./y) (Clift, 2006), with nearly 75% of material to the fan experiencing at least one glacial cycle of weathering onshore (Clift and Jonell, 2021b). The Pleistocene average reflects the net effect of periods of slower erosion and sediment transport during glacial periods and faster erosion during interglacial times. Modern fluxes may not be entirely representative of the natural river system (Milliman and Syvitski, 1992). Furthermore, the Indus River is presently greatly reduced in its discharge because of large scale irrigation in the upper flood plains reducing flow to the ocean (Inam et al., 2007), which may affect modern chemical weathering flux to the offshore. Pleistocene average sediment delivery rates of ~500–800 Mt./y for the BF (all models) derived from offshore volumes are moderately lower than that of the rivers, with modern gauged values closer to 520 and 540 Mt./y (Milliman and Syvitski, 1992; Lupker et al., 2011) for the Ganga and Brahmaputra rivers, respectively. Combined total estimates of ~1000 Mt./y are common (Coleman, 1969). Sediment fluxes derived from ^{10}Be sediment concentrations for the Ganga and Brahmaputra Rivers range higher up to 380–840 Mt./y and 780–1430 Mt./y, respectively, although it is recognized that centennially resolved ^{10}Be often yield apparent greater fluxes (Lupker et al., 2012a; Lupker et al., 2017).

The OC burial rates can also be compared with modern fluvial OC loads. The modern particulate OC export from the Mekong River is estimated at 0.27 Tmol/y (Galy et al., 2015), while average values since 1.8 Ma here are much lower at 0.032 Tmol/y. The Pearl River presently exports OC at a rate of 0.045 Tmol/y (Galy et al., 2015), compared with only 0.0053 Tmol/y estimated here. The difference is less for the Indus, which is estimated at 0.146 Tmol/y (Galy et al., 2015) compared to

Table 5
Summary carbon/CO_2 budget for all the depocentres considered in this work, showing the next results for all three models for the BF.

	Model 1				
Age (Ma)	Carbon reduction due to weathering (Tmol/y)	Mass of Org C buried (Tmol/y)	Total carbon sequestered (Tmol/y)	Organic carbon % of total consumption	% of Holocene consumption
1.80	0.86	0.53	1.39	38.1	11.9
2.58	0.89	0.34	1.23	27.4	10.5
3.60	0.73	0.30	1.03	28.8	8.8
5.33	0.60	0.23	0.83	27.9	7.1
7.25	0.62	0.25	0.87	29.2	7.5
10.50	0.56	0.20	0.76	26.3	6.5
10.90	0.56	0.20	0.76	26.1	6.5
11.63	0.44	0.13	0.57	22.5	4.8
13.00	0.52	0.16	0.68	23.4	5.8
13.82	0.53	0.14	0.67	20.6	5.7
14.80	0.54	0.13	0.67	19.9	5.7
15.50	0.54	0.13	0.67	19.6	5.7
15.97	0.53	0.15	0.68	22.4	5.8
17.00	0.45	0.12	0.57	21.3	4.9
18.00	0.45	0.07	0.52	13.8	4.4
19.50	0.44	0.07	0.51	13.9	4.3

	Model 2				
Age (Ma)	Carbon reduction due to weathering (Tmol/y)	Mass of Org C buried (Tmol/y)	Total carbon sequestered (Tmol/y)	Organic carbon % of total consumption	% of Holocene consumption
1.80	1.02	0.63	1.65	38.3	14.1
2.58	1.28	0.46	1.73	26.3	14.8
3.60	0.93	0.34	1.28	27.0	10.9
5.33	0.67	0.26	0.93	27.8	7.9
7.25	0.77	0.32	1.09	29.5	9.4
10.50	0.62	0.22	0.84	26.0	7.2
10.90	0.62	0.22	0.84	25.8	7.2
11.63	0.50	0.14	0.64	22.5	5.5
13.00	0.34	0.10	0.44	23.4	3.8
13.82	0.37	0.10	0.47	21.3	4.0
14.80	0.32	0.09	0.41	21.4	3.5
15.50	0.32	0.09	0.40	21.4	3.4
15.97	0.36	0.10	0.46	22.3	4.0
17.00	0.27	0.07	0.34	21.2	2.9
18.00	0.27	0.05	0.32	17.0	2.7
19.50	0.28	0.06	0.33	16.7	2.8

	Model 3				
Age (Ma)	Carbon reduction due to weathering (Tmol/y)	Mass of Org C buried (Tmol/y)	Total carbon sequestered (Tmol/y)	Organic carbon % of total consumption	% of Holocene consumption
1.80	0.67	0.41	1.08	37.8	9.3
2.58	0.68	0.27	0.95	28.5	8.1
3.60	0.52	0.25	0.77	31.9	6.6
5.33	0.41	0.16	0.58	28.3	4.9
7.25	0.71	0.30	1.01	29.4	8.7
10.50	0.66	0.23	0.88	25.8	7.6
10.90	0.66	0.23	0.88	25.6	7.6
11.63	0.53	0.15	0.69	22.5	5.9
13.00	0.73	0.22	0.95	23.3	8.1
13.82	0.74	0.19	0.93	20.2	8.0
14.80	0.75	0.18	0.93	19.2	7.9
15.50	0.76	0.18	0.93	18.8	8.0
15.97	0.73	0.21	0.94	22.4	8.0
17.00	0.46	0.13	0.59	21.3	5.0
18.00	0.46	0.07	0.54	13.6	4.6
19.50	0.45	0.07	0.53	13.7	4.5

0.095 Tmol/yr preserved since 1.8 Ma. The values are comparable in the Ganga-Brahmaputra, where OC export is 0.3 Tmol/y today (Galy et al., 2015), compared to values of 0.39 Tmol/y (Model 1), 0.49 Tmol/y (Model 2) and 0.27 Tmol/y (Model 3). These values from the BF would broadly support the idea that the BF is an efficient sink for OC in the geological record. The much lower values preserved in the Mekong and the Pearl River systems in the past could reflect anthropogenic disruption of the modern catchment, but also likely show the impact of decay of OC after export from the river delta and prior to burial and preservation on the seafloor. The sampling locations for both the Mekong and Pearl River systems are somewhat more distal relative to the river mouths than the Himalayan systems. Additionally, it is likely that the slower sedimentation rates offshore have a greater effect on OC decay and thus preservation than is true for the Himalayan submarine fans in the Indian Ocean.

6.4. Links to global climate change

If we consider the entire carbon budget, constructed here from combining the silicate chemical weathering and OC burial fluxes, a moderate increase in CO_2 sequestration initiated by the middle Miocene after 17 Ma (Fig. 9A-C). This is true regardless of which BF sedimentation model is favored; although the trend becomes more pronounced if the BF sedimentation rates are assumed to shadow the evolution of the Indus (Model 3). When compared relative to average global Holocene CO_2 consumption rates derived from rivers (11.7 Tmol/y; (Gaillardet et al., 1999)), silicate weathering and OC burial in Asian submarine fans reached levels equivalent to ~5% of this Holocene CO_2 level during the early Miocene, rising to 5–10% during the middle Miocene and 10–15% in the Pleistocene (Fig. 9B). The Model 3 budget would imply a peak of ~8% at 13 Ma, followed by a fall, and rising again to a maximum value of 9.3% in the Pleistocene. Models 1 and 2 predict higher maximum proportions of 11.9% and 14.1%, respectively.

When compared to global Neogene seawater temperatures (Westerhold et al., 2020) and atmospheric CO_2 concentrations (Rae et al., 2021), the rise in the influence of the South Asian fans over global CO_2 concentrations coincided with the beginning of the Miocene Climatic Optimum (MCO)(Fig. 9D) and peak Neogene CO_2 levels (Fig. 9E). Because greater CO_2 sequestration driven by silicate weathering is expected to cause cooling rather than warming of global climate, we infer that warmer global temperatures at this time enhanced the total silicate weathering flux of the Himalayan area (Wan et al., 2009; Clift and Jonell, 2021a). Falling global temperatures following the MCO are paralleled by generally steady CO_2 consumption rates related in part to silicate weathering documented by fan deposits (Fig. 9A). This is the opposite of what is predicted for the Himalayan uplift-erosion-weathering hypothesis. Only Model 2 shows a modest increase in CO_2 consumption rates after the MCO (~15 Ma; Fig. 8 and 9A), as would be predicted.

The early-middle Miocene was a time of rapidly evolving plate kinematics in Asia, including dynamic mountain uplift resulting from break-off of the subducting Indian Plate beneath the Himalaya and SE Tibetan Plateau (Mugnier and Huyghe, 2006; Webb et al., 2017). Recent work highlights the dual role of uplifting mountains in driving the global carbon budget; as CO_2 consumers as explored in detail here but also as significant sources of CO_2 through carbonate and pyrite weathering (Bufe et al., 2021; Zondervan et al., 2023). Enhanced erosion of the carbonate-rich Tethyan Himalaya could potentially overwhelm the silicate weathering impact, as might be expected under the faster silicate erosion documented here. Carbonate, pyrite and OC weathering processes offset silicate weathering processes, although a net budget is not achievable with the data presented here. Falling relative erosion from the more mafic Karakoram and Kohistan in the Indus since the Miocene would reduce the reactivity of sediments reaching the IF (Zhou et al., 2021b), although increasing mafic material sourced to the BF after 4–3 Ma has been observed (Fig. 3E)(Blum et al., 2018).

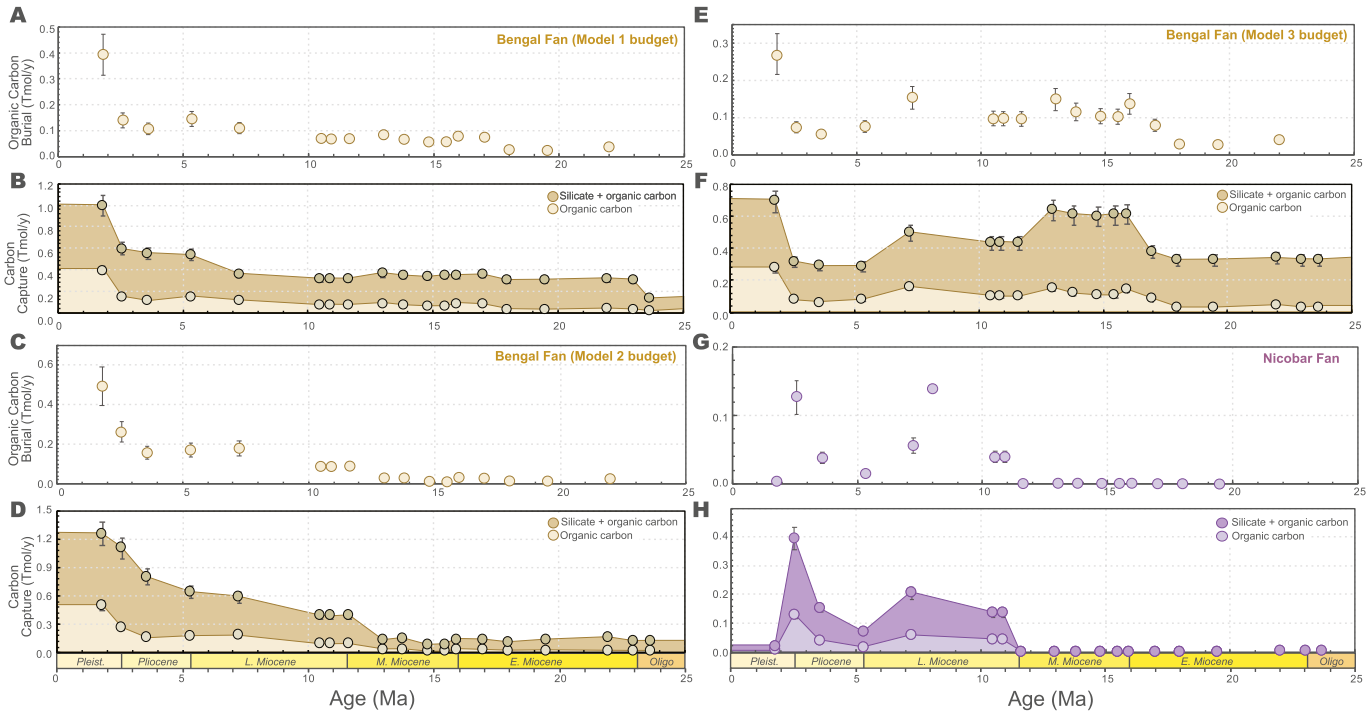

Fig. 6. Plot showing temporal evolution in A) stacked, cumulative OC flux and B) OC, silicate weathering related carbon capture and total carbon capture for the BF using the sediment budget based on regional seismic from the western BoB (Model 1), C) and D are using the sediment budget based on ODP Site 758 (Model 2), E) and F) are using the sediment budget mirroring the Indus Fan (Model 3), and G) and H) are for the Nicobar Fan.

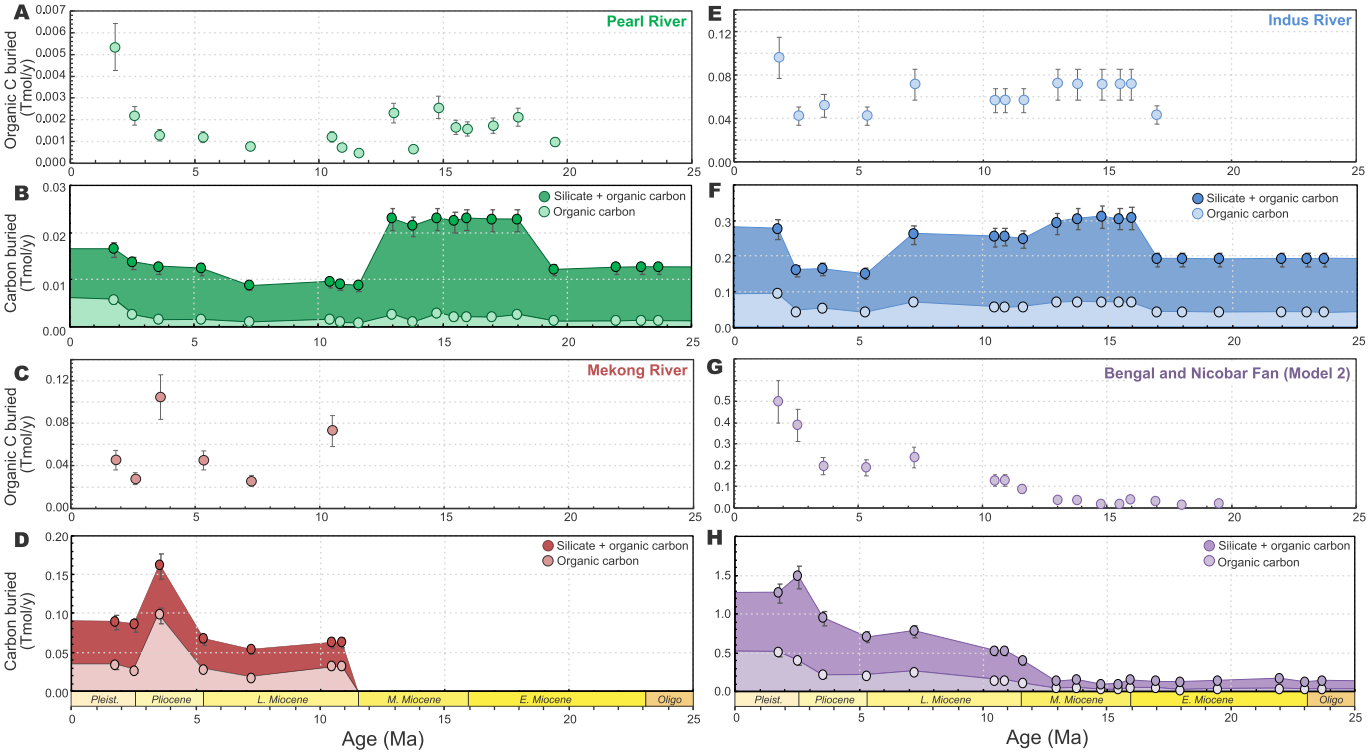

Fig. 7. Plot showing temporal evolution in A) stacked, cumulative OC flux and B) OC, chemical weathering related carbon capture and total carbon capture for the Pearl River, C) and D for the Mekong River, E) and F) are for the Indus Fan, and G) and H) are for the combined BF and Nicobar Fan based on sedimentation Model 2.

It is only during the Plio-Pleistocene that rising rates of CO_2 sequestration from Asian fan silicate weathering and OC burial correlate with global cooling, as predicted by the uplift-erosion-weathering hypothesis (Raymo and Ruddiman, 1992). Any influence of this region on global temperature is likely restricted to the last ~5 m.y. OC represents ~15–20% of the total regional carbon budget in the early Miocene (Fig. 9C), after which OC rose to >20% after 17 Ma and then >30% of the total regional carbon budget in the Pliocene (Table 5). This

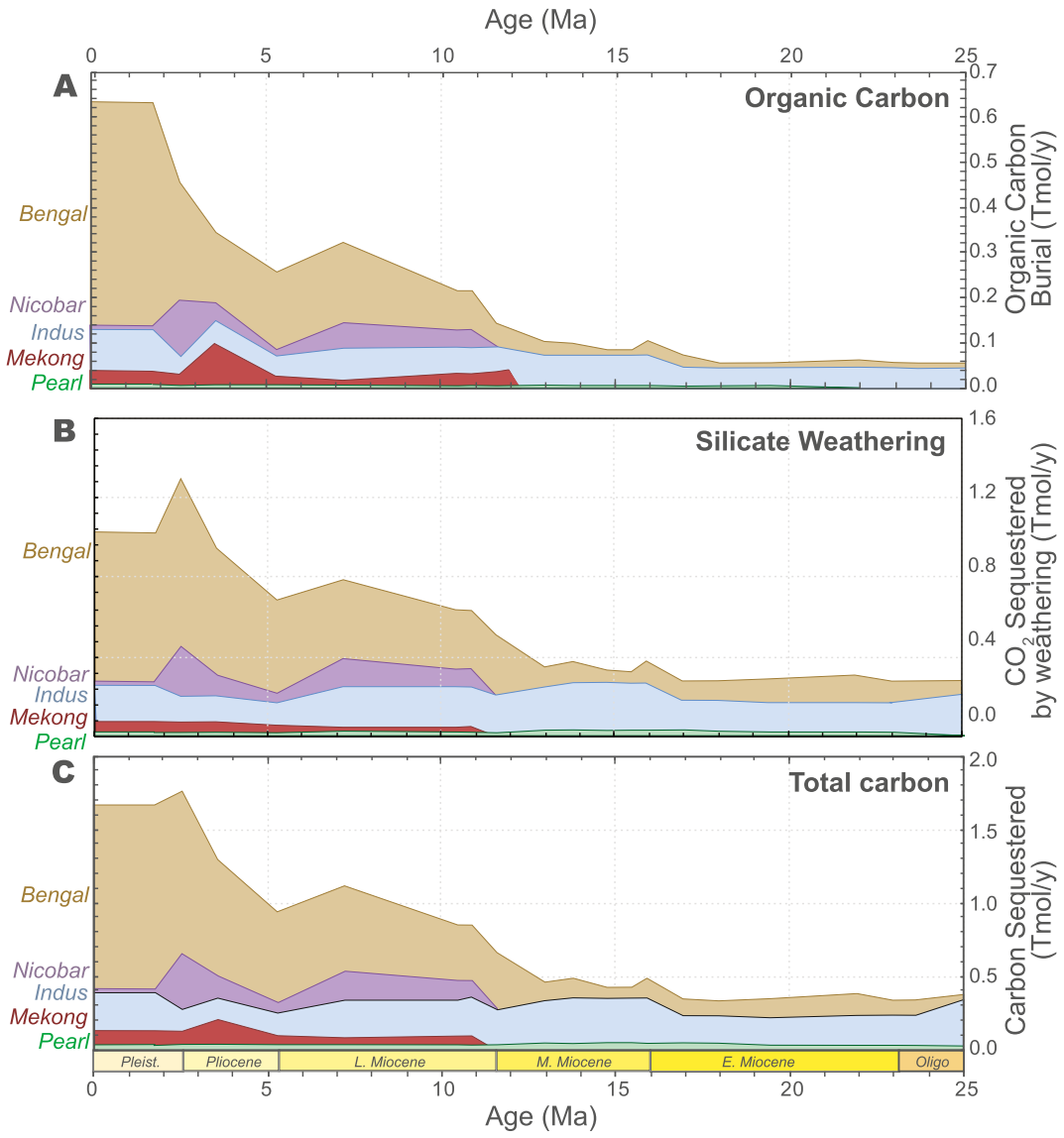

Fig. 8. Temporal evolution in A) the burial of OC in the deep sea depocentres analyzed in this study. B) the carbon sequestered due to consumption of CO_2 by chemical weathering. C) total carbon removed. BF estimates are based on the ODP Site 758-proxied mass accumulation rate.

increasing importance likely reflects progressively more efficient OC burial and preservation offshore, especially within the BF (Figs. 6 and 9C).

6.5. Links with the Asian monsoon

Regional climate is expected to partly control carbon sequestration in Asia because both OC productivity and silicate weathering rates are linked to temperature and humidity (West et al., 2005). Likewise, Neogene CO_2 drawdown in Himalayan catchments caused by silicate weathering and OC burial does not appear to be linked solely with global temperature over the period of interest, at least during the Miocene when silicate weathering flux increases with temperature (Figs. 9A and D). If the regional carbon budget presented here is compared to reconstructed Asian Summer Monsoon rainfall intensity (Clift et al., 2008), rising carbon consumption by silicate weathering and OC burial broadly correlates with increasing physical erosion linked to the rainfall intensity across the region peaking at 15.5–17 Ma under a tropical 'ever-wet' regime rather than a seasonal monsoonal regime (Fig. 9F) (Yang et al., 2020). Strong summer monsoon conditions from 15 to 11 Ma in the middle Miocene occur during a time of global cooling, alongside steady (or decreasing in Model 3) CO_2 consumption by silicate weathering and OC burial. Analysis of hemipelagic sediment on the Ninety East Ridge showed weaker chemical weathering intensity starting in the middle Miocene as the cooling began and the monsoon climate dried (Ali et al., 2021). It is the faster erosion proposed by Models 1 and 2 at this time that increased reactivity and allows chemical weathering fluxes to be maintained (Caves Rugenstein et al., 2019). Steady CO_2 consumption during continued cooling could imply additional controls on silicate weathering and OC burial than temperature alone. It may be partly caused by sustained monsoon intensity even during post-MCO cooling (Fig. 9F). Falling sedimentation rates during the mid-late Miocene caused moderate decreases in silicate weathering and OC fluxes in the IF and more in the Pearl River (Fig. 7)(Clift and Jonell, 2021a).

Clay mineral data from Asian marginal seas support a more intense weathering regime in the warm and wet Miocene (Clift et al., 2014; Liu et al., 2017; Zhou et al., 2021a), followed by either steady chemical weathering relative to physical weathering, or slightly decreased chemical weathering (Ali et al., 2021). Peaks in physical erosion recorded across South and East Asian seas suggest strong monsoonal conditions across Asia increased physical weathering during the middle Miocene (Wan et al., 2007; Clift et al., 2008; Shen et al., 2017; Ali et al.,

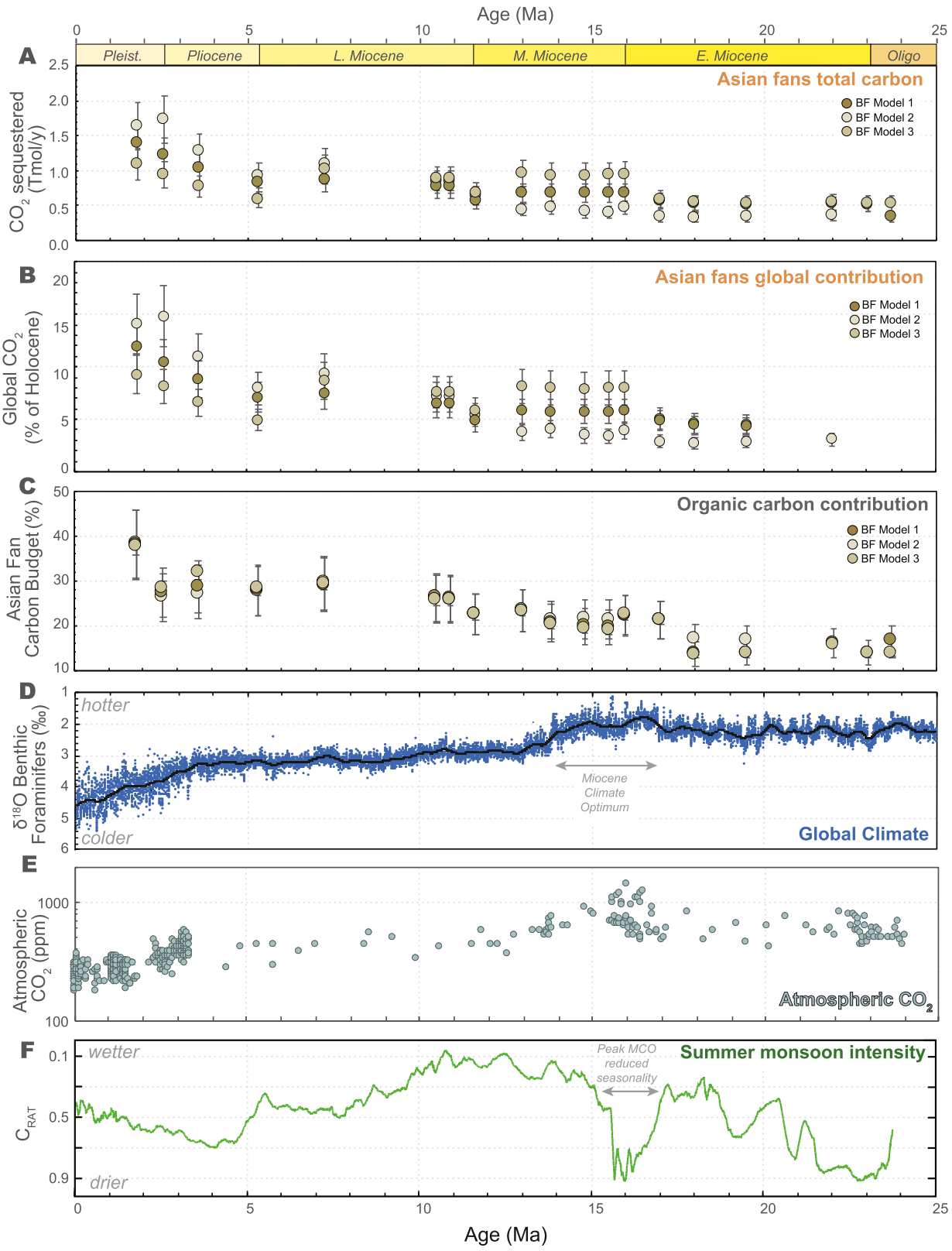

Fig. 9. A) Temporal evolution in the percent of total carbon sequestered by all the deep sea depocentres compared to the Holocene average showing the difference resulting from using a BF sediment budget based in ODP Site 758 and if the BF mirrors the Indus. B) Temporal development in the impact of Asian weathering on global CO_2 concentrations, relative to the Holocene pre-industrial average. C) Temporal development in the relative importance of OC to the total carbon budgets of the deep sea depocentres. D) Global climate proxied by benthic foraminiferal oxygen isotopes (Westerhold et al., 2020). E) Atmospheric CO_2 levels from Rae et al. (2021), F) Asian monsoon intensity proxied by the clay-related C_{RAT} proxy from South China Sea (Clift et al., 2008). The high C_{RAT} values during the MCO (light blue) indicate low seasonality rather than dry conditions. (For interpretation of the references to colour in this figure legend, the reader is referred to the web version of this article.)

2021). Between the late Miocene (post-8 Ma) and before the middle Pliocene, monsoon weakening coincides with falling to arguably steady carbon consumption by Asian fans and broadly decreasing atmospheric CO_2. A weakening monsoon would result in slower physical erosion and overall, less intense silicate weathering, as well as slower petrogenic OC, pyrite- and carbonate weathering at this time. The monsoon may have dominated if reduced net release of CO_2 drove the long-term global cooling trend at this time.

Strong monsoons appear to not necessarily drive increased CO_2 consumption by OC burial. OC burial reached a maximum in the Pleistocene but never dominated the regional carbon sink or consumption budget considered here. Silicate chemical weathering in Asia, rather than OC burial, contributed substantially to the global carbon budget but did not solely drive Neogene global cooling trends. Only during the Plio-Pleistocene does OC burial become more important to the total carbon budget and a possible control on global climate. Alternatively, weathering elsewhere, possibly in tropical SE Asia and Oceania (Park et al., 2020; Bayon et al., 2023; Martin et al., 2023), or changes in mantle degassing (Herbert et al., 2022) may have driven Neogene atmosphere CO_2 levels over million-year timescales. Erosion of the Himalaya, Gangdese and Karakoram supplying the BF and IF, rather than erosion of the Tibetan Plateau supplying the Mekong and Pearl, are the primary bedrock 'consumers' in terms of regional carbon sequestration because material derived from those terranes comprises the majority of weathered sediment held in the deep-sea.

7. Conclusions

Atmospheric CO_2 is one of the primary controls over the long-term evolution of Earth climate and represents the long-term balance between solid Earth and the atmosphere inputs and outputs. Mountain building has long been understood to induce the removal of atmospheric CO_2 through silicate weathering processes but now is increasingly recognized to also release CO_2 to the atmosphere. Petrogenic OC and carbonate weathering, aided by the breakdown of rock-derived pyrite, can offset or even exceed the influence of silicate breakdown on atmospheric CO_2 (Horan et al., 2019; Bufe et al., 2021; Zondervan et al., 2023). In this study, we quantified CO_2 sequestration driven by silicate mineral breakdown and burial of organic carbon (OC) in the major depocenters linked to the building of the Himalaya and Tibetan Plateau. We compiled whole rock major element data from silty sediment cored from the submarine fans of the Indian Ocean and South China Sea, together with their OC contents, and integrated these with a seismically-defined sediment flux budget to quantify the amount of CO_2 sequestration. In this reassessment, we find that OC contributes less to the CO_2 budget than previously estimated (<30%), except during the Pleistocene when there was enhanced physical erosion and rapid OC burial. Broadly, preservation of OC in the geological record is significantly lower than that exported in the modern Asian river systems because of the OC decomposition on the seafloor prior to burial. Despite its significant volume, we show that Bengal Fan sediment silicate weathering processes are less efficient there than in other Himalayan-Tibetan Plateau river systems. The more reactive bedrock composition of the source regions in the Indus and Mekong rivers aids in more efficient CO_2 consumptions over the Neogene.

We highlight that rates of erosion and sediment delivery to deep-sea fans remain the most important variables controlling long-term silicate weathering fluxes, yet significant obstacles remain in constructing reliable mass flux budgets. Even so, the volumetrically large Bengal Fan is still by far the largest contributor to the regional Asian fan carbon budget, especially since the middle Miocene Climatic Optimum (17–15 Ma). Prior to that time, the Indus Fan controlled the regional CO_2 budget, largely because of faster erosion occurring in its onshore catchment. We observe increased silicate chemical weathering fluxes during the MCO driven by global temperature (high CO_2) and a very strong monsoon. Strong monsoon conditions persisted through much of the Miocene and sustained steady CO_2 consumption by Asian fans. Continued trends in mid-late Miocene global cooling require additional regions and/or processes controlling global CO_2 beyond the erosion and weathering of Himalaya-Tibetan silicates and burial of OC. Only until after ~5–3 Ma does the sequestration of CO_2 via Asian fans, primarily by rapid burial of OC, appear to strongly influence or positively feedback on global trends in CO_2 and climate.

CRediT authorship contribution statement

Peter D. Clift: Conceptualization, Formal analysis, Investigation, Methodology, Project administration, Supervision, Validation, Visualization, Writing – original draft. **Tara N. Jonell:** Formal analysis, Methodology, Supervision, Validation, Visualization, Writing – original draft. **Yifan Du:** Validation, Visualization, Writing – original draft. **Thomas Bornholdt:** Data curation, Writing – review & editing.

Declaration of competing interest

The authors declare that they have no known competing financial interests or personal relationships that could have appeared to influence the work reported in this paper.

Data availability

The data is either published or included in the manuscript

Acknowledgments

PC acknowledges support from the Charles T. McCord Jr. Chair in Petroleum Geology at LSU and advice from Shiming Wan and Christian France-Lanord. This manuscript benefited from comments by editor Oleg Pokrovsky, Robert Hilton and two anonymous reviewers.

References

Ali, S., Hathorne, E.C., Frank, M., 2021. Persistent Provenance of South Asian Monsoon-Induced Silicate Weathering over the past 27 Million Years. Paleoceanogr. Paleoclimatol. 36 (3), e2020PA003909 https://doi.org/10.1029/2020PA003909.

Alizai, A., Carter, A., Clift, P.D., VanLaningham, S., Williams, J.C., Kumar, R., 2011. Sediment provenance, reworking and transport processes in the Indus River by U-Pb dating of detrital zircon grains. Glob. Planet. Chang. 76, 33–55. https://doi.org/10.1016/j.gloplacha.2010.11.008.

Alt, J.C., Teagle, D.A.H., 1999. The uptake of carbon during alteration of ocean crust. Geochim. Cosmochim. Acta 63 (10), 1527–1535. https://doi.org/10.1016/S0016-7037(99)00123-4.

Bach, W., Peucker-Ehrenbrink, B., Hart, S.R., Blusztajn, J.S., 2003. Geochemistry of hydrothermally altered oceanic crust: DSDP/ODP Hole 504B – Implications for seawater-crust exchange budgets and Sr- and Pb-isotopic evolution of the mantle. Geochem. Geophys. Geosyst. 4 (3) https://doi.org/10.1029/2002GC000419.

Bayon, G., Patriat, M., Godderis, Y., Trinquier, A., De Deckker, P., Kulhanek, D.K., Holbourn, A., Rosenthal, Y., 2023. Accelerated mafic weathering in Southeast Asia linked to late Neogene cooling. Sci. Adv. 9 (13), eadf3141 https://doi.org/10.1126/sciadv.adf3141.

Berner, R.A., Berner, E.K., 1997. Silicate weathering and climate. In: Ruddiman, W.F. (Ed.), Tectonic Uplift and Climate Change. Springer, New York, pp. 353–365.

Bhattacharjee, S., Bookhagen, B., Sinha, R., Wieser, A., Marchhart, O., 2023. 26Al and 10Be concentrations from alluvial drill cores across the Indo-Gangetic plain reveal multimillion-year sediment-transport lag times. Earth Planet. Sci. Lett. 619, 118318 https://doi.org/10.1016/j.epsl.2023.118318.

Blum, M., Rogers, K., Gleason, J., Najman, Y., Cruz, J., Fox, L., 2018. Allogenic and Autogenic Signals in the Stratigraphic Record of the Deep-Sea Bengal Fan. Sci. Rep. 8 (1), 7973. https://doi.org/10.1038/s41598-018-25819-5.

Bouilhol, P., Jagoutz, O., Hanchar, J.M., Dudas, F.O., 2013. Dating the India-Eurasia collision through arc magmatic records. Earth Planet. Sci. Lett. 366, 163–175.

Brady, P.V., Gíslason, S.R., 1997. Seafloor weathering controls on atmospheric CO2 and global climate. Geochim. Cosmochim. Acta 61 (5), 965–973. https://doi.org/10.1016/S0016-7037(96)00385-7.

Bufe, A., Hovius, N., Emberson, R., Rugenstein, J.K.C., Galy, A., Hassenruck-Gudipati, H. J., Chang, J.-M., 2021. Co-variation of silicate, carbonate and sulfide weathering drives CO2 release with erosion. Nat. Geosci. 14 (4), 211–216. https://doi.org/10.1038/s41561-021-00714-3.

Caldeira, K., 1995. Long-term control of atmospheric carbon dioxide; low-temperature seafloor alteration or terrestrial silicate-rock weathering? Am. J. Sci. 295 (9), 1077–1114. https://doi.org/10.2475/ajs.295.9.1077.

Calmels, D., Gaillardet, J.R.M., Brenot, A.S., France-Lanord, C., 2007. Sustained sulfide oxidation by physical erosion processes in the Mackenzie River basin: Climatic perspectives. Geology 35 (11), 1003–1006. https://doi.org/10.1130/g24132a.1.
Castelltort, S., Van Den Driessche, J., 2003. How plausible are high-frequency sediment supply-driven cycles in the stratigraphic record? Sediment. Geol. 157, 3–13.
Caves, J.K., Jost, A.B., Lau, K.V., Maher, K., 2016. Cenozoic carbon cycle imbalances and a variable weathering feedback. Earth Planet. Sci. Lett. 450, 152–163. https://doi.org/10.1016/j.epsl.2016.06.035.
Caves Rugenstein, J.K., Ibarra, D.E., von Blanckenburg, F., 2019. Neogene cooling driven by land surface reactivity rather than increased weathering fluxes. Nature 571 (7763), 99–102. https://doi.org/10.1038/s41586-019-1332-y.
Chabaux, F., Blaes, E., Granet, M., Roupert, R.D.C., Stille, P., 2012. Determination of transfer time for sediments in alluvial plains using 238U-234U-230Th disequilibria: the case of the Ganges river system. Compt. Rendus Geosci. 344 (11), 688–703. https://doi.org/10.1016/j.crte.2012.10.013.
Clift, P.D., 2002. A brief history of the Indus River. In: Clift, P.D., Kroon, D., Gaedicke, C., Craig, J. (Eds.), The Tectonic and Climatic Evolution of the Arabian Sea Region. Special Publications, vol. 195. Geological Society, London, pp. 237–258. https://doi.org/10.1144/GSL.SP.2002.195.01.13.
Clift, P.D., 2006. Controls on the erosion of Cenozoic Asia and the flux of clastic sediment to the ocean. Earth Planet. Sci. Lett. 241 (3–4), 571–580. https://doi.org/10.1016/j.epsl.2005.11.028.
Clift, P.D., Giosan, L., 2014. Sediment fluxes and buffering in the post-glacial Indus Basin. Basin Res. 26, 369–386. https://doi.org/10.1111/bre.12038.
Clift, P.D., Jonell, T.N., 2021a. Himalayan-Tibetan Erosion is not the Cause of Neogene Global Cooling. Geophys. Res. Lett. 48 (8), e2020GL087742 https://doi.org/10.1029/2020GL087742.
Clift, P.D., Jonell, T.N., 2021b. Monsoon controls on sediment generation and transport: Mass budget and provenance constraints from the Indus River catchment, delta and submarine fan over tectonic and multi-millennial timescales. Earth Sci. Rev. 220, 103682 https://doi.org/10.1016/j.earscirev.2021.103682.
Clift, P.D., Shimizu, N., Layne, G., Gaedicke, C., Schlüter, H.U., Clark, M.K., Amjad, S., 2001. Development of the Indus Fan and its significance for the erosional history of the western Himalaya and Karakoram. Geol. Soc. Am. Bull. 113, 1039–1051. https://doi.org/10.1130/0016-7606(2001)113<1039:DOTIFA>2.0.CO;2.
Clift, P.D., Hodges, K., Heslop, D., Hannigan, R., Hoang, L.V., Calves, G., 2008. Correlation of Himalayan exhumation rates and Asian monsoon intensity. Nat. Geosci. 1, 875–880. https://doi.org/10.1038/ngeo351.
Clift, P.D., Wan, S., Blusztajn, J., 2014. Reconstructing Chemical Weathering, Physical Erosion and Monsoon Intensity since 25 Ma in the northern South China Sea: a review of competing proxies. Earth Sci. Rev. 130, 86–102. https://doi.org/10.1016/j.earscirev.2014.01.002.
Clift, P.D., Zhou, P., Stockli, D.F., Blusztajn, J., 2019. Regional Pliocene exhumation of the Lesser Himalaya in the Indus drainage. Solid Earth 10, 647–661. https://doi.org/10.5194/se-10-647-2019.
Clift, P.D., Betzler, C., Clemens, S.C., Christensen, B., Eberli, G.P., France-Lanord, C., Gallagher, S., Holbourn, A., Kuhnt, W., Murray, R.W., Rosenthal, Y., Tada, R., Wan, S., 2022. A synthesis of monsoon exploration in the Asian marginal seas. Sci. Drill. 10, 1–29. https://doi.org/10.5194/sd-10-1-2022.
Cochran, J.R., Stow, D.A.V., Shipboard Scientific Party, 1989. Proceedings of the Ocean Drilling Program, Initial Reports. Ocean Drilling Program, College Station, TX. https://doi.org/10.2973/odp.proc.ir.116.1989.
Coleman, J.M., 1969. Brahmaputra river: Channel processes and sedimentation. Sediment. Geol. 3 (2), 129–239. https://doi.org/10.1016/0037-0738(69)90010-4.
Coogan, L.A., Gillis, K.M., 2013. Evidence that low-temperature oceanic hydrothermal systems play an important role in the silicate-carbonate weathering cycle and long-term climate regulation. Geochem. Geophys. Geosyst. 14 (6), 1771–1786. https://doi.org/10.1002/ggge.20113.
Crowley, T.J., Berner, R.A., 2001. CO2 and climate Change. Science 292, 870–872. https://doi.org/10.1126/science.1061664.
Curray, J.R., Emmel, F.J., Moore, D.G., 2003. The Bengal Fan: morphology, geometry, stratigraphy, history and processes. Mar. Pet. Geol. 19, 1191–1223.
Derry, L., France-Lanord, C., 1997. Himalayan weathering and erosion fluxes; climate and tectonic controls. In: Ruddiman, W.F. (Ed.), Tectonic Uplift and Climate Change. Plenum Press, New York, pp. 289–312.
Dessert, C., Dupré, B., Francois, L.M., Schott, J., Gaillardet, J., Chakrapani, G., Bajpai, S., 2001. Erosion of Deccan Traps determined by river geochemistry: impact on the global climate and the 87Sr/86Sr ratio of seawater. Earth Planet. Sci. Lett. 188, 459–474.
Dunlea, A.G., Murray, R.W., Santiago Ramos, D.P., Higgins, J.A., 2017. Cenozoic global cooling and increased seawater Mg/Ca via reduced reverse weathering. Nat. Commun. 8 (1), 844. https://doi.org/10.1038/s41467-017-00853-5.
Exnicios, E.M., Carter, A., Najman, Y., Clift, P.D., 2022. Late Miocene unroofing of the Inner Lesser Himalaya recorded in the NW Himalaya foreland basin. Basin Res. 34 (6), 1894–1916. https://doi.org/10.1111/bre.12689.
France-Lanord, C., Derry, L.A., 1997. Organic carbon burial forcing of the carbon cycle from Himalayan erosion. Nature 390, 65–67.
France-Lanord, C., Derry, L., Michard, A., 1993. Evolution of the Himalaya since Miocene time: Isotopic and sedimentologic evidence from the Bengal Fan. In: Treloar, P.J., Searle, M.P. (Eds.), Himalayan Tectonics. Special Publications, vol. 74. Geological Society, London, pp. 603–621.
France-Lanord, C., Galy, V., Pik, R., Singh, S.K., 2006. Extreme erosion of the Eastern Himalayan syntaxis traced by isotopic compositions of river and bengal fan sediments. EOS Trans. Am. Geophys. Union 87, T32B–03.
France-Lanord, C., Spiess, V., Klaus, A., Shipboard Scientific Party, 2016b. Site U1451. In: Proceedings of the International Ocean Discovery Program, vol. 354. https://doi.org/10.14379/iodp.proc.354.105.2016.
France-Lanord, C., Spiess, V., Klaus, A., Schwenk, T., 2016a. Expedition 354 Scientists. In: Bengal Fan. Proceedings of the International Ocean Discovery Program. International Ocean Discovery Program, College Station, TX. https://doi.org/10.14379/iodp.proc.354.2016.
Gabet, E.J., Burbank, D.W., Pratt-Sitaula, B., Putkonen, J., Bookhagen, B., 2008. Modern erosion rates in the High Himalayas of Nepal. Earth Planet. Sci. Lett. 267 (3), 482–494. https://doi.org/10.1016/j.epsl.2007.11.059.
Gaillardet, J., Dupré, B., Louvat, P., Allègre, C.J., 1999. Global silicate weathering and CO2 consumption rates deduced from the chemistry of large rivers. Chem. Geol. 159 (1–4), 3–30.
Galy, A., France-Lanord, C., 1999. Weathering processes in the Ganges-Brahmaputra basin and the riverine alkalinity budget. Chem. Geol. 159 (1–4), 31–60.
Galy, V., France-Lanord, C., Beyssac, O., Faure, P., Kudrass, H.-R., Palhol, F., 2007. Efficient organic carbon burial in the Bengal fan sustained by the Himalayan erosional system. Nature 450, 407–411. https://doi.org/10.1038/nature06273.
Galy, V., Beyssac, O., France-Lanord, C., Eglinton, T., 2008. Recycling of graphite during Himalayan erosion: a geological stabilisation of C in the crust. Science 322, 943–945.
Galy, V., Peucker-Ehrenbrink, B., Eglinton, T., 2015. Global carbon export from the terrestrial biosphere controlled by erosion. Nature 521 (7551), 204–207. https://doi.org/10.1038/nature14400.
GEBCO Compilation Group, 2019. The GEBCO_2019 grid - a continuous terrain model of the global oceans and land. In: N.O.C (Ed.), British Oceanographic Data Centre. https://doi.org/10.5285/836f016a-33be-6ddc-e053-6c86abc0788e.
Gradstein, F.M., Ogg, J.G., Schmitz, M.D., Ogg, G.M., 2020. Geologic Time Scale 2020. Elsevier Science, p. 1358 (ISBN: 9780128243619).
Granet, M., Chabaux, F., Stille, P., Dosseto, A., France-Lanord, C., Blaes, E., 2010. U-series disequilibria in suspended river sediments and implication for sediment transfer time in alluvial plains: the case of the Himalayan rivers. Geochim. Cosmochim. Acta 74 (10), 2851–2865. https://doi.org/10.1016/j.gca.2010.02.016.
Grujic, D., Coutand, I., Bookhagen, B., Bonnet, S.P., Blythe, A., Duncan, C., 2006. Climatic forcing of erosion, landscape, and tectonics in the Bhutan Himalayas. Geology 34 (10), 801–804. https://doi.org/10.1130/g22648.1.
Gudasz, C., Bastviken, D., Steger, K., Premke, K., Sobek, S., Tranvik, L.J., 2010. Temperature-controlled organic carbon mineralization in lake sediments. Nature 466 (7305), 478–481. https://doi.org/10.1038/nature09186.
Herbert, T.D., Dalton, C.A., Liu, Z., Salazar, A., Si, W., Wilson, D.S., 2022. Tectonic degassing drove global temperature trends since 20 Ma. Science 377 (6601), 116–119. https://doi.org/10.1126/science.abl4353.
Hilton, R.G., Gaillardet, J., Calmels, D., Birck, J.-L., 2014. Geological respiration of a mountain belt revealed by the trace element rhenium. Earth Planet. Sci. Lett. 403, 27–36. https://doi.org/10.1016/j.epsl.2014.06.021.
Hilton, R.G., Turowski, J.M., Winnick, M., Dellinger, M., Schleppi, P., Williams, K.H., Lawrence, C.R., Maher, K., West, M., Hayton, A., 2021. Concentration-discharge relationships of dissolved rhenium in Alpine catchments reveal its use as a tracer of oxidative weathering. Water Resour. Res. 57 (11), e2021WR029844 https://doi.org/10.1029/2021WR029844.
van Hinsbergen, D.J.J., Lippert, P.C., Dupont-Nivet, G., McQuarrie, N., Doubrovine, P.V., Spakman, W., Torsvik, T.H., 2012. Greater India Basin hypothesis and a two-stage Cenozoic collision between India and Asia. Proc. Natl. Acad. Sci. 109 (20), 7659–7664. https://doi.org/10.1073/pnas.1117262109.
Hodges, K.V., 2000. Tectonics of the Himalaya and southern Tibet from two perspectives. Geol. Soc. Am. Bull. 112 (3), 324–350.
Holeman, J.N., 1968. The Sediment Yield of Major Rivers of the World. Water Resour. Res. 4 (4), 737–747. https://doi.org/10.1029/WR004i004p00737.
Horan, K., Hilton, R.G., Dellinger, M., Tipper, E., Galy, V., Calmels, D., Selby, D., Gaillardet, J., Ottley, C.J., Parsons, D.R., Burton, K.W., 2019. Carbon dioxide emissions by rock organic carbon oxidation and the net geochemical carbon budget of the Mackenzie River Basin. Am. J. Sci. 319 (6), 473. https://doi.org/10.2475/06.2019.02.
Huyan, Y., Zhang, B., Wang, X., Lu, Y., Liu, F., 2023. Geochemistry of the Lancang River (Upper Mekong River) overbank sediments: Implications for provenance, weathering and sedimentary characteristics. Appl. Geochem. 156, 105747 https://doi.org/10.1016/j.apgeochem.2023.105747.
Huyghe, P., Bernet, M., Galy, A., Naylor, M., Cruz, J., Gyawali, B.R., Gemignani, L., Mugnier, J.L., 2020. Rapid exhumation since at least 13 Ma in the Himalaya recorded by detrital apatite fission-track dating of Bengal fan (IODP Expedition 354) and modern Himalayan river sediments. Earth Planet. Sci. Lett. 534, 116078 https://doi.org/10.1016/j.epsl.2020.116078.
Inam, A., Clift, P.D., Giosan, L., Tabrez, A.R., Tahir, M., Rabbani, M.M., Danish, M., 2007. The geographic, geological and oceanographic setting of the Indus River. In: Gupta, A. (Ed.), Large Rivers: Geomorphology and Management. John Wiley and Sons, Chichester, UK, pp. 333–345.
Isson, T.T., Planavsky, N.J., 2018. Reverse weathering as a long-term stabilizer of marine pH and planetary climate. Nature 560 (7719), 471–475. https://doi.org/10.1038/s41586-018-0408-4.
Jagoutz, O., Macdonald, F.M., Royden, L., 2016. Low-latitude arc–continent collision as a driver for global cooling. Proc. Natl. Acad. Sci. 113 (18), 4935–4940. https://doi.org/10.1073/pnas.1523667113.
Jin, H., Wan, S., Clift, P.D., Liu, C., Huang, J., Jiang, S., Li, M., Qin, L., Shi, X., Li, A., 2022. Birth of the Pearl River at 30 Ma: evidence from sedimentary records in the northern South China Sea. Earth Planet. Sci. Lett. 600, 117872 https://doi.org/10.1016/j.epsl.2022.117872.

Jin, H., Wan, S., Liu, C., Zhao, D., Pei, W., Yu, Z., Zhang, J., Song, Z., Li, M., Tang, Y., Li, A., 2023. Evolution of silicate weathering in South China since 30 Ma: Controlling factors and global implications. Glob. Planet. Chang. 223, 104095 https://doi.org/10.1016/j.gloplacha.2023.104095.

Krishna, K.S., Ismaiel, M., Srinivas, K., Rao, D.G., Mishra, J., Saha, D., 2016. Sediment pathways and emergence of Himalayan source material in the Bay of Bengal. Curr. Sci. 110 (3), 363–372.

Kump, L.R., Arthur, M.A., 1997. Global chemical erosion during the Cenozoic: Weatherability balances the budget. In: Ruddiman, W.F. (Ed.), Tectonics, Uplift and Climate Change. Plenum Publishing Co., New York, pp. 399–426.

Lavé, J., Avouac, J.P., 2001. Fluvial incision and tectonic uplift across the Himalaya of Central Nepal. J. Geophys. Res. 106, 26,561–26,592. https://doi.org/10.1029/2001JB000359.

Lee, H., Galy, V., Feng, X., Ponton, C., Galy, A., France-Lanord, C., Feakins, S.J., 2019. Sustained wood burial in the Bengal Fan over the last 19 My. Proc. Natl. Acad. Sci. 116 (45), 22518–22525. https://doi.org/10.1073/pnas.1913714116.

Lehner, B., Grill, G., 2013. Global river hydrography and network routing: baseline data and new approaches to study the world's large river systems. Hydrol. Process. 27 (15), 2171–2186. https://doi.org/10.1002/hyp.9740.

Lehner, B., Verdin, K., Jarvis, A., 2008. New global hydrography derived from spaceborne elevation data. EOS Trans. Am. Geophys. Union 89 (10), 93–94. https://doi.org/10.1029/2008EO100001.

Lenard, S.J.P., Lavé, J., France-Lanord, C., Aumaître, G., Bourlès, D.L., Keddadouche, K., 2020. Steady erosion rates in the Himalayas through late Cenozoic climatic changes. Nat. Geosci. 13 (6), 448–452. https://doi.org/10.1038/s41561-020-0585-2.

Li, C.-F., Lin, J., Kulhanek, D.K., Williams, T., Bao, R., Briais, A., Brown, E.A., Chen, Y., Clift, P.D., Colwell, F.S., Dadd, K.A., Ding, W., Almeida, I.H., Huang, X.-L., Hyun, S., Jiang, T., Koppers, A.A.P., Li, Q., Liu, C., Liu, Q., Liu, Z., Nagai, R.H., Peleo-Alampay, A., Su, X., Sun, Z., Tejada, M.L.G., Trinh, H.S., Yeh, Y.-C., Zhang, C., Zhang, F., Zhang, G.-L., Zhao, X., 2015. Site U1433. In: Proceedings of the International Ocean Discovery Program, vol. 349. https://doi.org/10.14379/iodp.proc.349.105.2015.

Li, S., Lu, X.X., Bush, R.T., 2014. Chemical weathering and CO2 consumption in the lower Mekong River. Sci. Total Environ. 472, 162–177. https://doi.org/10.1016/j.scitotenv.2013.11.027.

Li, S.-L., Calmels, D., Han, G., Gaillardet, J., Liu, C.-Q., 2008. Sulfuric acid as an agent of carbonate weathering constrained by δ13CDIC: examples from Southwest China. Earth Planet. Sci. Lett. 270 (3), 189–199. https://doi.org/10.1016/j.epsl.2008.02.039.

Liu, C., Clift, P.D., Murray, R.W., Blusztajn, J., Ireland, T., Wan, S., Ding, W., 2017. Geochemical evidence for Initiation of the Modern Mekong Delta in the southwestern South China Sea after 8 Ma. Chem. Geol. 451, 38–54. https://doi.org/10.1016/j.chemgeo.2017.01.008.

Lupker, M., France-Lanord, C., Lavé, J., Bouchez, J., Galy, V., Métivier, F., Gaillardet, J., Lartiges, B., Mugnier, J.L., 2011. A Rouse-based method to integrate the chemical composition of river sediments: application to the Ganga basin. J. Geophys. Res. 116 (F04012) https://doi.org/10.1029/2010JF001947.

Lupker, M., Blard, P.-H., Lavé, G., Christian France-Lanord, Laetitia Leanni, Nicolas Puchol, Julien Charreau, Bourles, D., 2012a. 10Be-derived Himalayan denudation rates and sediment budgets in the Ganga basin. Earth Planet. Sci. Lett. 333–334, 146–156. https://doi.org/10.1016/j.epsl.2012.04.020.

Lupker, M., France-Lanord, C., Galy, V., Lave, J., Gaillardet, J., Gajured, A.P., Guilmette, C., Rahman, M., Singh, S.K., Sinha, R., 2012b. Predominant floodplain over mountain weathering of Himalayan sediments (Ganga basin). Geochim. Cosmochim. Acta 84, 410–432.

Lupker, M., Lavé, J., France-Lanord, C., Christl, M., Bourlès, D., Carcaillet, J., Maden, C., Wieler, R., Rahman, M., Bezbaruah, D., Xiaohan, L., 2017. 10Be systematics in the Tsangpo-Brahmaputra catchment: the cosmogenic nuclide legacy of the eastern Himalayan syntaxis. Earth Surf. Dynam. 5 (3), 429–449. https://doi.org/10.5194/esurf-5-429-2017.

Macdonald, F.A., Swanson-Hysell, N.L., Park, Y., Lisiecki, L., Jagoutz, O., 2019. Arc-continent collisions in the tropics set Earth's climate state. Science 364 (6436), 181–184. https://doi.org/10.1126/science.aav5300.

Mackenzie, F.T., Kump, L.R., 1995. Reverse weathering, clay mineral formation, and oceanic element cycles. Science 270 (5236), 586–587. https://doi.org/10.1126/science.270.5236.586.

Maffre, P., Swanson-Hysell, N.L., Goddéris, Y., 2021. Limited carbon cycle response to increased sulfide weathering due to oxygen feedback. Geophys. Res. Lett. 48 (19), e2021GL094589 https://doi.org/10.1029/2021GL094589.

Martin, P.E., Macdonald, F.A., McQuarrie, N., Flowers, R.M., Maffre, P.J.Y., 2023. The rise of New Guinea and the fall of Neogene global temperatures. Proc. Natl. Acad. Sci. 120 (40), e2306492120 https://doi.org/10.1073/pnas.2306492120.

McNeill, L.C., Dugan, B., Backman, J., Pickering, K.T., Pouderoux, H.F.A., Henstock, T.J., Petronotis, K.E., Carter, A., Chemale, F., Milliken, K.L., Kutterolf, S., Mukoyoshi, H., Chen, W., Kachovich, S., Mitchison, F.L., Bourlange, S., Colson, T.A., Frederik, M.C. G., Guèrin, G., Hamahashi, M., House, B.M., Hüpers, A., Jeppson, T.N., Kenigsberg, A.R., Kuranaga, M., Nair, N., Owari, S., Shan, Y., Song, I., Torres, M.E., Vannucchi, P., Vrolijk, P.J., Yang, T., Zhao, X., Thomas, E., 2017a. Understanding Himalayan erosion and the significance of the Nicobar Fan. Earth Planet. Sci. Lett. 475, 134–142. https://doi.org/10.1016/j.epsl.2017.07.019.

McNeill, L.C., Dugan, B., Petronotis, K.E., Expedition 362 Scientists, 2017b. Sumatra Subduction Zone. In: Proceedings of the International Ocean Discovery Program, vol. 362. https://doi.org/10.14379/iodp.proc.362.2017.

McNeill, L.C., Dugan, B., Petronotis, K.E., Shipboard Scientific Party, 2017c. Site U1480. In: Proceedings of the International Ocean Discovery Program, 362. https://doi.org/10.14379/iodp.proc.362.103.2017.

Métivier, F., Gaudemer, Y., Tapponnier, P., Klein, M., 1999. Mass accumulation rates in Asia during the Cenozoic. Geophys. J. Int. 137 (2), 280–318.

Meybeck, M., 1976. Total mineral dissolved transport by world major rivers. Hydrol. Sci. Bull. XXI (2), 265–284.

Milliman, J.D., Syvitski, J.P.M., 1992. Geomorphic/tectonic control of sediment discharge to the ocean; the importance of small mountainous rivers. J. Geol. 100, 525–544.

Misra, S., Froelich, P.N., 2012. Lithium Isotope history of Cenozoic Seawater: changes in Silicate Weathering and reverse Weathering. Science 335 (6070), 818–823. https://doi.org/10.1126/science.1214697.

Mugnier, J.-L., Huyghe, P., 2006. Ganges basin geometry records a pre-15 Ma isostatic rebound of Himalaya. Geology 34 (6), 445–448. https://doi.org/10.1130/G22089.1.

Najman, Y., 2006. The detrital record of orogenesis: a review of approaches and techniques used in the Himalayan sedimentary basins. Earth Sci. Rev. 74 (1–2), 1–72.

Najman, Y., Appel, E., Boudagher-Fadel, M., Bown, P., Carter, A., Garzanti, E., Godin, L., Han, J., Liebke, U., Oliver, G., Parrish, R., Vezzoli, G., 2010. Timing of India-Asia collision: Geological, biostratigraphic, and palaeomagnetic constraints. J. Geophys. Res. 115 https://doi.org/10.1029/2010JB007673.

Nesbitt, H.W., Markovics, G., Price, R.C., 1980. Chemical processes affecting alkalis and alkaline earths during continental weathering. Geochim. Cosmochim. Acta 44, 1659–1666.

Pande, K., Sarin, M.M., Trivedi, J.R., Krishnaswami, S., Sharma, K.K., 1994. The Indus river system (India-Pakistan): major-ion chemistry, uranium and strontium isotopes. Chem. Geol. 116 (3), 245–259. https://doi.org/10.1016/0009-2541(94)90017-5.

Pandey, D.K., Clift, P.D., Kulhanek, D.K., Andò, S., Bendle, J.A.P., Bratenkov, S., Griffith, E.M., Gurumurthy, G.P., Hahn, A., Iwai, M., Khim, B.-K., Kumar, A., Kumar, A.G., Liddy, H.M., Lu, H., Lyle, M.W., Mishra, R., Radhakrishna, T., Routledge, C.M., Saraswat, R., Saxena, R., Scardia, G., Sharma, G.K., Singh, A.D., Steinke, S., Suzuki, K., Tauxe, L., Tiwari, M., Xu, Z., Yu, Z., 2016a. Site U1456. In: Proceedings of the International Ocean Discovery Program, 355. https://doi.org/10.14379/iodp.proc.355.103.2016.

Pandey, D.K., Clift, P.D., Kulhanek, D.K., Andò, S., Bendle, J.A.P., Bratenkov, S., Griffith, E.M., Gurumurthy, G.P., Hahn, A., Iwai, M., Khim, B.-K., Kumar, A., Kumar, A.G., Liddy, H.M., Lu, H., Lyle, M.W., Mishra, R., Radhakrishna, T., Routledge, C.M., Saraswat, R., Saxena, R., Scardia, G., Sharma, G.K., Singh, A.D., Steinke, S., Suzuki, K., Tauxe, L., Tiwari, M., Xu, Z., Yu, Z., 2016b. Site U1457. In: Proceedings of the International Ocean Discovery Program, 355. https://doi.org/10.14379/iodp.proc.355.104.2016.

Park, Y., Maffre, P., Goddéris, Y., Macdonald, F.A., Anttila, E.S.C., Swanson-Hysell, N.L., 2020. Emergence of the Southeast Asian islands as a driver for Neogene cooling. Proc. Natl. Acad. Sci. 117 (41), 25319–25326. https://doi.org/10.1073/pnas.2011033117.

Pickering, K.T., Carter, A., Andò, S., Garzanti, E., Limonta, M., Vezzoli, G., Milliken, K.L., 2020. Deciphering relationships between the Nicobar and Bengal submarine fans, Indian Ocean. Earth Planet. Sci. Lett. 544, 116329 https://doi.org/10.1016/j.epsl.2020.116329.

Prins, M.A., Postma, G., Cleveringa, J., Cramp, A., Kenyon, N.H., 2000. Controls on terrigenous sediment supply to the Arabian Sea during the late Quaternary: the Indus Fan. Mar. Geol. 169, 327–349. https://doi.org/10.1016/S0025-3227(00)00086-4.

Rae, J.W.B., Zhang, Y.G., Liu, X., Foster, G.L., Stoll, H.M., Whiteford, R.D.M., 2021. Atmospheric CO2 over the past 66 Million Years from Marine Archives. Annu. Rev. Earth Planet. Sci. 49 (1), 609–641. https://doi.org/10.1146/annurev-earth-082420-063026.

Raymo, M.E., Ruddiman, W.F., 1992. Tectonic forcing of late Cenozoic climate. Nature 359 (6391), 117–122. https://doi.org/10.1038/359117a0.

Repasch, M., Scheingross, J.S., Hovius, N., Lupker, M., Wittmann, H., Haghipour, N., Gröcke, D.R., Orfeo, O., Eglinton, T.I., Sachse, D., 2021. Fluvial organic carbon cycling regulated by sediment transit time and mineral protection. Nat. Geosci. 14 (11), 842–848. https://doi.org/10.1038/s41561-021-00845-7.

Richter, F.M., Rowley, D.B., DePaolo, D.J., 1992. Sr isotope evolution of seawater; the role of tectonics. Earth Planet. Sci. Lett. 109, 11–23. https://doi.org/10.1016/0012-821X(92)90070-C.

Rothman, D.H., Forney, D.C., 2007. Physical model for the decay and preservation of marine organic carbon. Science 316 (5829), 1325–1328. https://doi.org/10.1126/science.1138211.

Routledge, C.M., Kulhanek, D.K., Tauxe, L., Scardia, G., Singh, A.D., Steinke, S., Griffith, E.M., Saraswat, R., 2020. Revised geological timescale for IODP Sites U1456 and U1457. Geol. Mag. 157 (6), 961–978. https://doi.org/10.1017/S0016756819000104.

Rudnick, R.L., Gao, S., 2003. The composition of the continental crust. In: Rudnick, R.L. (Ed.), The Crust. Treatise on Geochemistry, 3. Elsevier-Pergamon, Oxford, pp. 1–64.

Searle, M.P., Law, R.D., Jessup, M., Simpson, R.L., 2006. Crustal structure and evolution of the Greater Himalaya in Nepal – South Tibet: Implications for channel flow and ductile extrusion of the middle crust. In: Law, R.D., Searle, M.P., Godin, L. (Eds.), Channel Flow, Ductile Extrusion and Exhumation in Continental Collision Zones. Special Publication, vol 268. Geological Society, London, pp. 355–378.

Shackleton, N.J., 1987. The carbon isotope record of the Cenozoic: history of organic carbon burial and of oxygen in the ocean and atmosphere. In: Brooks, J., Fleet, A.J. (Eds.), Marine Petroleum Source Rocks. Special Publications, vol. 26. Geological Society, London, pp. 423–434. https://doi.org/10.1144/GSL.SP.1987.026.01.27.

Shen, X., Wan, S., France-Lanord, C., Clift, P.D., Tada, R., Révillon, S., Shi, X., Zhao, D., Liu, Y., Yin, X., Song, Z., Li, A., 2017. History of Asian eolian input to the Sea of Japan since 15 Ma: Links to Tibetan uplift or global cooling? Earth Planet. Sci. Lett. 474, 296–308. https://doi.org/10.1016/j.epsl.2017.06.053.

Shipboard Scientific Party, 1989. Site 718. In: Cochran, J.R., Stow, D.A.V. (Eds.), Proceedings of the Ocean Drilling Program, Part A: Initial Reports, vol. 116. Ocean Drilling Program, College Station, TX, pp. 91–154.

de Sigoyer, J., Chavagnac, V., Blichert-Toft, J., Villa, I.M., Luais, B., Guillot, S., Cosca, M., Mascle, G., 2000. Dating the Indian continental subduction and collisional thickening in the Northwest Himalaya; multichronology of the Tso Morari eclogites. Geology 28 (6), 487–490.

Singh, M., Sharma, M., Tobschall, H.J., 2005. Weathering of the Ganga alluvial plain, northern India: implications for fluvial geochemistry of the Gomati river. Applied Geochemistry 20, 1–21. https://doi.org/10.1016/j.apgeochem.2004.07.005.

Sobek, S., Durisch-Kaiser, E., Zurbrügg, R., Wongfun, N., Wessels, M., Pasche, N., Wehrli, B., 2009. Organic carbon burial efficiency in lake sediments controlled by oxygen exposure time and sediment source. Limnol. Oceanogr. 54 (6), 2243–2254. https://doi.org/10.4319/lo.2009.54.6.2243.

Song, Z., Wan, S., Colin, C., France-Lanord, C., Yu, Z., Dapoigny, A., Jin, H., Li, M., Zhang, J., Zhao, D., Shi, X., Li, A., 2023. Enhanced weathering input from South Asia to the Indian Ocean since the late Eocene. Sci. Bull. https://doi.org/10.1016/j.scib.2023.01.015.

Spence, J., Telmer, K., 2005. The role of sulfur in chemical weathering and atmospheric CO2 fluxes: evidence from major ions, δ13CDIC, and δ34SSO4 in rivers of the Canadian Cordillera. Geochim. Cosmochim. Acta 69 (23), 5441–5458. https://doi.org/10.1016/j.gca.2005.07.011.

Suchet, P.A., Probst, J.-L., Ludwig, W., 2003. Worldwide distribution of continental rock lithology: Implications for the atmospheric/soil CO2 uptake by continental weathering and alkalinity river transport to the oceans. Glob. Biogeochem. Cycles 1 (2), 1038–1051. https://doi.org/10.1029/2002gb001891.

Summerfield, M., Hulton, N.J., 1994. Natural controls of fluvial denudaiton rates in major world drainage basins. J. Geophys. Res. 99 (B7), 13871–13883.

Tachambalath, A.P., France-Lanord, C., Galy, A., Rigaudier, T., Charreau, J., 2023. Data report: major and trace element composition of silicates and carbonates from Bengal Fan sediments, IODP Expedition 354. Proceed. Intern. Ocean Discov. Progr. 354, 1–10. https://doi.org/10.14379/iodp.proc.354.204.2023.

Torres, M.A., West, A.J., Li, G., 2014. Sulphide oxidation and carbonate dissolution as a source of CO2 over geological timescales. Nature 507 (7492), 346–349. https://doi.org/10.1038/nature13030.

Touret, J.L., 1992. CO2 transfer between the upper mantle and the atmosphere: temporary storage in the lower continental crust. Terra Nova 4 (1), 87–98. https://doi.org/10.1111/j.1365-3121.1992.tb00453.x.

Vögeli, N., van der Beek, P., Huyghe, P., Najman, Y., 2017. Weathering in the Himalaya, an East-West comparison: indications from major elements and clay mineralogy. J. Geol. 125, 515–529. https://doi.org/10.1086/692652.

Walker, J.C.G., Hays, P.B., Kasting, J.F., 1981. A negative feedback mechanism for the long-term stabilization of Earth's surface temperature. J. Geophys. Res. Oceans 86 (C10), 9776–9782. https://doi.org/10.1029/JC086iC10p09776.

Wan, S., Li, A., Clift, P.D., Stuut, J.-B.W., 2007. Development of the East Asian monsoon: Mineralogical and sedimentologic records in the northern South China Sea since 20 Ma. Palaeogeogr. Palaeoclimatol. Palaeoecol. 254 (3–4), 561–582. https://doi.org/10.1016/j.palaeo.2007.07.009.

Wan, S., Kürschner, W.M., Clift, P.D., Li, A., Li, T., 2009. Extreme weathering / erosion during the Miocene Climatic Optimum: evidence from sediment record in the South China Sea. Geophys. Res. Lett. 36 (L19706) https://doi.org/10.1029/2009GL040279.

Wang, P., Prell, W.L., Blum, P., Shipboard Scientific Party, 2000. Site 1148. In: Proceedings of the Ocean Drilling Program, Part A: Initial Reports, vol. 184, p. 121. https://doi.org/10.2973/odp.proc.ir.184.109.2000.

Webb, A.A.G., Guo, H., Clift, P.D., Husson, L., Müller, T., Costantino, D., Yin, A., Xu, Z., Cao, H., Wang, Q., 2017. The Himalaya in 3D: Slab dynamics controlled mountain building and monsoon intensification. Lithosphere. https://doi.org/10.1130/L636.1.

Weber, M.E., Wiedicke-Hombach, M., Kudrass, H.R., Erlenkeuser, H., 2003. Bengal Fan sediment transport activity and response to climate forcing inferred from sediment physical properties. Sediment. Geol. 155 (3), 361–381. https://doi.org/10.1016/S0037-0738(02)00187-2.

West, A.J., Galy, A., Bickle, M.J., 2005. Tectonic and climatic controls on silicate weathering. Earth Planet. Sci. Lett. 235, 211–228. https://doi.org/10.1016/j.epsl.2005.03.020.

Westerhold, T., Marwan, N., Drury, A.J., Liebrand, D., Agnini, C., Anagnostou, E., Barnet, J.S.K., Bohaty, S.M., De Vleeschouwer, D., Florindo, F., Frederichs, T., Hodell, D.A., Holbourn, A.E., Kroon, D., Lauretano, V., Littler, K., Lourens, L.J., Lyle, M., Pälike, H., Röhl, U., Tian, J., Wilkens, R.H., Wilson, P.A., Zachos, J.C., 2020. An astronomically dated record of Earth's climate and its predictability over the last 66 million years. Science 369 (6509), 1383–1387. https://doi.org/10.1126/science.aba6853.

Willenbring, J.K., von Blanckenburg, F., 2010. Long-term stability of global erosion rates and weathering during late-Cenozoic cooling. Nature 465, 211–214. https://doi.org/10.1038/nature09044.

Wulf, H., Bookhagen, B., Scherler, D., 2010. Seasonal precipitation gradients and their impact on fluvial sediment flux in the Northwest Himalaya. Geomorphology 118 (1), 13–21. https://doi.org/10.1016/j.geomorph.2009.12.003.

Xu, Z., Liu, C.-Q., 2010. Water geochemistry of the Xijiang basin rivers, South China: Chemical weathering and CO2 consumption. Appl. Geochem. 25 (10), 1603–1614 doi:0.1016/j.apgeochem.2010.08.012.

Yang, X., Groeneveld, J., Jian, Z., Steinke, S., Giosan, L., 2020. Middle miocene intensification of South Asian Monsoonal rainfall. Paleoceanogr. Paleoclimatol. 35 (12), e2020PA003853 https://doi.org/10.1029/2020PA003853.

Zhou, P., Ireland, T., Murray, R.W., Clift, P.D., 2021a. Marine sedimentary records of chemical weathering evolution in the Western Himalaya since 17 Ma. Geosphere 17 (3), 824–853. https://doi.org/10.1130/GES02211.1.

Zhou, P., Stockli, D.F., Ireland, T., Murray, R.W., Clift, P.D., 2021b. Zircon U-Pb age constraints on NW Himalayan exhumation from the Laxmi Basin, Arabian Sea. Geochem. Geophys. Geosyst. 23 (1), e2021GC010158 https://doi.org/10.1029/2021GC010158.

Zondervan, J.R., Hilton, R.G., Dellinger, M., Clubb, F.J., Roylands, T., Ogrič, M., 2023. Rock organic carbon oxidation CO2 release offsets silicate weathering sink. Nature. https://doi.org/10.1038/s41586-023-06581-9.